Journal of Hydrology 586 (2020) 124905

Contents lists available at ScienceDirect

Journal of Hydrology

journal homepage: www.elsevier.com/locate/jhydrol

Research papers

A review of remote sensing applications in agriculture for food security: Crop growth and yield, irrigation, and crop losses

L. Karthikeyan[a,b], Ila Chawla[c], Ashok K. Mishra[b,*]

[a] Centre of Studies in Resources Engineering, IIT Bombay, Powai, Mumbai, India
[b] Department of Civil Engineering, Clemson, SC, USA
[c] Interdisciplinary Centre for Water Research (ICWaR), Indian Institute of Science, Bangalore, India

ARTICLE INFO

This manuscript was handled by G. Syme, Editor-in-Chief

Keywords:
Agriculture
Remote sensing
Crop yield
Data assimilation
Irrigation
Crop losses

ABSTRACT

The global population is expected to reach 9.8 billion by 2050. There is an exponential growth of food production to meet the needs of the growing population. However, the limited land and water resources, climate change, and an increase in extreme events likely to pose a significant threat for achieving the sustainable agriculture goal. Given these challenges, food security is included in the United Nations' Sustainable Development Goals (SDGs). Since the advent of Sputnik, followed by the Explorer missions, satellite remote sensing is assisting us in collecting the data at global scales. In this work, we review how satellite remote sensing information is utilized to assess and manage agriculture, an important component of ecohydrology. Overall, three critical aspects of agriculture are considered: (a) crop growth and yield through empirical models, physics-based models, and data assimilation in crop models, (b) applications pertaining to irrigation, which include mapping irrigation areas and quantification of irrigation, and (c) crop losses due to pests, diseases, crop lodging, and weeds. The emphasis is on satellite sensors in optical, thermal, microwave, and fluorescence frequencies. We conclude the review with an outlook of challenges and recommendations. This paper is the first of a two-part review series. The second part reviews the role of satellite remote sensing in water security, wherein we discuss the aspects of water quality and quantity along with extremes (floods and droughts).

1. Introduction

The global food security is recognized as a part of the Sustainable Development Goals (SDGs; SDG2 in particular) by the United Nations (United Nations, 2015) through an increase in sustainable agriculture production, a decrease in food losses and waste, improved nutrition, and ensuring zero hunger. Over the past few decades, the global population has exceeded 7.5 billion, with the majority of the population residing in the urban areas (Klein Goldewijk et al. 2010). However, according to USDA (https://www.usda.gov/topics/food-and-nutrition/food-security), 700 million people across 76 countries are still food insecure. The increasing population has put immense pressure on food and water resources. Global food production must increase by 50% to meet the demands of the projected world population by 2050 (Chakraborty and Newton 2011; Godfray et al. 2010; Tilman et al. 2011). To ensure food security for the growing population, there has been a dramatic expansion in the cropland areas and the irrigation water requirement (Tilman et al. 2011). From 1961 to 2004, the total area under cultivation increased by 2.3 times globally (http://faostat.fao.org/). The irrigated cropland areas increased from 63 million Ha (MHa) in 1900 to 306 MHa in 2005 globally (Siebert et al. 2015). The irrigated agricultural areas are estimated to use around two-third of the total water reserves globally, which accounts for about 80–90% of the total water consumption (Doell et al. 2014; Oki and Kanae 2006; Shiklomanov and Rodda 2004).

Despite the expansion in agricultural areas, food security may continue to be a problem in the developing nations due to improper management of resources and policies related to the pricing of food and irrigation water use (Calzadilla et al. 2013; Easterling and Apps 2005; Scholes and Biggs 2004). The effects of anthropogenic climate change may further influence the crop yield, thereby hampering the management of the food and water systems in the near future (Easterling and Apps 2005). The extreme events such as floods and droughts strongly influence the four factors, namely, availability of food, access to safe food, food prices, and the sustainable food utilization, which regulate the global food security (Brown et al. 2015). The changing climate conditions can induce prolonged droughts in the future, which can increase the crop dependency on groundwater resources for irrigation,

* Corresponding author.
E-mail address: ashokm@g.clemson.edu (A.K. Mishra).

https://doi.org/10.1016/j.jhydrol.2020.124905

Available online 30 March 2020

thereby affecting their sustainability (Scanlon et al. 2012). The reminiscence of these effects is already evident through an increase in the groundwater depletion globally from 1960 to 2000 (Wada et al. 2010). Climate change can also lead to a reversal of croplands from irrigated to rainfed agricultural systems, which can significantly impact food production (Elliott et al. 2014). The deficit in irrigation may result in wilting of plants, which ultimately reduces the crop yield.

On the other hand, excess irrigation can also impede the crop growth in the forms of lack of sufficient air for respiration (thereby affecting the germination of seeds), increase in salinity due to evaporation of standing water and crop lodging (Chen et al., 2011; Wichelns and Qadir, 2015). Apart from these factors, pests and diseases may significantly reduce crop productivity (Oerke 2006), further adding to the global food insecurity. Besides, the recent changes in the dietary requirements and production of biofuels on the croplands have added to the existing pressure on the food resources (Godfray et al. 2010). Therefore, given the growing food demands and changing climate, wise management of depleting water resources through improved irrigation and storage provisions along with flood/drought resistance crop varieties may contribute towards sustainable agriculture practices and maintain food security (Carruthers et al. 1997; Ozdogan 2011).

1.1. *Necessity of satellite remote sensing*

Food security is a broad subject and requires monitoring of several indicators, such as crop growth and crop yield, irrigation, and the spread of diseases. To achieve this, direct or indirect measurement of several variables in space–time is required. Satellite remote sensing, in addition to the in-situ observation network, is being increasingly used to provide information on these variables at multiple spatial and temporal scales, independent of geopolitical boundaries. Although the insitu data is most accurate, their spatial coverage is inadequate and it is often expensive to deploy radars and sensors to improve their spatiotemporal resolutions, especially in developing countries. The remotely sensed data is often used to retrieve variations in the vegetation state by providing realistic information on photosynthesis, phenology, disturbances, recovery, and human interventions. This information is critical for determining crop health and productivity and serves as an essential measure for agriculture planning and management.

As discussed earlier, food security is intrinsically affected by the water cycle. Water cycle, in turn, receives feedback from vegetation as transpiration. The objective of this study is to review the satellite remote sensing for sustainable agriculture management as well as some recent developments that have taken place to monitor and improve crop management. This review can be characterized under the broad spectrum of ecohydrology, which studies about soil water-plant interactions along with plant water stress and productivity (Hsiao, 1973; Nilsen & Orcutt, 1996; Vico & Porporato, 2015). Food production is the biggest anthropogenic consumer of water (D'Odorico et al., 2010). So, besides understanding the process of irrigation (which is directly related to the field of water resources), it is also important to study the crop productivity and the associated stresses. Three important aspects are addressed in this review, 1) monitoring crop growth and yield assessment, 2) qualitative and quantitative assessment of irrigation, and 3) detecting crop losses due to pests, diseases, crop lodging, and weeds. Fig. 1 presents a detailed schematic diagram of these selected areas and the sub-topics reviewed in this work. This review is the first of the two-part review series, wherein the second part reviews the applications of satellite remote sensing for water security, which includes the aspects of water quality, quantity, and extreme events (Chawla et al., 2020). Section 2 presents an overview of satellite remote sensing along with a list of satellites, which find applications in this review. Section 3 presents a review of the three selected areas. Section 4 presents the outlook of this review.

2. Overview of satellite remote sensing

Satellite remote sensing emerged as a successor of aerial remote sensing during the 1960 s with the Explorer, TIROS (Television Infrared Observation Satellite) series, Corona, and later with Landsat missions, among others (Lettenmaier et al., 2015). The process of remote sensing is initiated with electromagnetic radiations from the Sun (passive remote sensing) or from the satellite itself (active remote sensing). The incident radiations are reflected, absorbed and transmitted while interacting with the Earth's surface. The satellite sensor measures these reflected radiations, which contain information about the terrestrial processes taking place during the overpass of the satellite at a location. The terrestrial processes include the components of the hydrological cycle, vegetation processes, interactions with water bodies, geomorphology, and topography. Each of the terrestrial processes could be sensitive to measurements in only specific wavelengths/frequencies. So, it is essential to identify the satellite sensors that are appropriate for the purpose. Furthermore, the satellite measurements are also influenced by spatial, temporal, spectral and radiometric resolutions, which are associated with sensor configuration.

Satellites sensors record the reflected radiations across various wavelengths of the electromagnetic spectrum. These wavelengths typically range from visible/optical spectrum (0.4–0.7 μm wavelength); infrared spectrum – consisting of three bands, near infrared (NIR) (0.7–1.3 μm wavelength), mid infrared (MIR) (1.3–3.0 μm wavelength), and thermal infrared (TIR) (3.0–14 μm wavelength); and microwave spectrum (1 mm-1 m wavelength). In this section, we present a list of satellite sensors that belong to the optical/thermal spectrum (Table 1), microwave spectrum – which are categorized under active microwave sensors (Table 2) and passive microwave sensors (Table 3), and gravity field sensors (Table 4). These tables also contain information on duration, spatial and temporal resolutions of satellite sensors.

3. Remote sensing for food security

Agriculture is one of the essential sectors to support the livelihood of humans and livestock. Its growth is imperative for the growth of the economy and the alleviation of poverty. With the advent of technology and improvements in pesticides and fertilizers, modern agricultural practices have significantly increased crop yields compared to that of traditional agricultural practices (Hazell and Wood 2007). Satellite remote sensing provides efficient means to monitor agriculture at large spatial scales. The following sections present remote sensing applications in three aspects of food security, crop growth assessment, irrigation, and crop losses.

3.1. *Crop growth assessment*

Crop yield is generally used to represent the outcome of agriculture. It is defined as the weight of crop output (e.g., grain, fruit) at certain soil moisture content per unit harvested area of the crop (Fischer 2015). Crop yield is dependent on meteorological conditions, water and nutrient availability, and the amount of absorbed photosynthetically active radiation (aPAR). Crops should be supplied with the above inputs and protected from pests and diseases in order to produce expected yield. In this process, there is a need for continuous monitoring of crop growth. Here we present the critical variables necessary to monitor crop growth.

The aPAR of the crop depends on the incoming solar radiation and the crop's photosynthetically active radiation interception capability, which is mainly influenced by the leaf area (Rembold et al. 2013). Besides, the fraction of absorbed photosynthetically active radiation (fPAR), a widely used variable, normalizes aPAR with the amount of incident solar radiation. The fPAR further influences a) Gross Primary Productivity (GPP) – the rate at which plant absorbs the incident radiation during the photosynthesis, and b) Net Primary Productivity

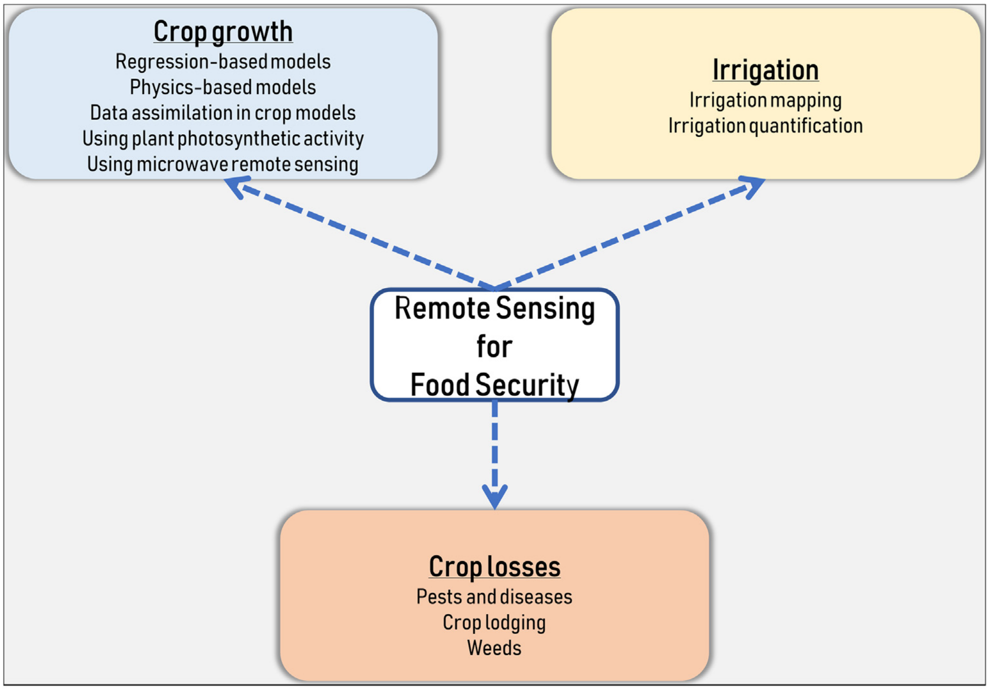

Fig. 1. Schematic diagram of the review of the role of remote sensing applications for agriculture management.

(NPP) – the rate at which the absorbed energy is stored as plant biomass. GPP and NPP are expressed in the units of weight of carbon per unit area per unit time (generally $gC/m^2/yr$). The GPP, in a way, measures the accumulated photosynthesis during the crop growth. Both crop yield and crop biomass are measured as weight per area (generally kg/hectare or tons/hectare). The Light Use Efficiency (LUE) is the efficiency with which the plant converts aPAR to NPP ($NPP = aPAR \times LUE$) (Monteith 1977).

The Leaf Area Index (LAI), defined as the ratio between the one-sided green leaf area and ground surface area, is used to assess the leaf characteristics and crop biomass (Mulla 2013). It influences the canopy reflectance. Typically, LAI ranges between 0 (bare ground) to more than 10 (evergreen coniferous forests) (Iio et al. 2014). Recently, Solar Induced Chlorophyll Fluorescence (SIF), an indicator of plant photosynthetic activity, is used to study plant productivity (Guanter et al. 2014). The indicators discussed here are widely used to study plant growth with remote sensing (Bartlett et al. 1988; Fassnacht et al. 1997; Shibayama et al. 1993; Thenkabail et al. 1994; Wiegand and Richardson 1990). The methods to estimate these indicators using remote sensing information can be classified broadly into three categories: 1) regression-based methods, 2) physics-based methods.

3.1.1. Regression-based methods

Remote sensing of crop yield relies on crop spectral properties, which vary according to the growth stage of the crop, type of crop, and its health. During the 1970 s, field and airborne remote sensing campaigns are conducted to monitor the vegetation and crop yield (Collins 1978; Tucker, 1979; Tucker and Maxwell 1976). These efforts have resulted in the development of vegetation indices, which are functions of spectral reflectance from specific wavelengths (recorded by the remote sensor). Specifically, the vegetation is found to be very reflective and absorptive in the near infra-red (NIR) and red bands. Therefore, some combination of these reflectivities from these two bands will be sensitive to the vegetation dynamics (Sellers 1987; Tucker, 1979). Among these indices, Normalized Difference Vegetation Index (NDVI) (Rouse et al., 1974) is perhaps the most widely used index to monitor vegetation health and dynamics. Given its strong relationship with LAI and fraction of absorbed PAR (fPAR; the ratio between absorbed PAR and incident PAR), NDVI can be related to crop yield (Baret and Guyot 1991; Groten 1993; Prince 1991). In addition to NDVI, some more vegetation indices are proposed in the past in order to address the issues about atmospheric effects and canopy background, among others (Gitelson 2004). Some of them include Enhanced Vegetation Index (EVI) (Liu and Huete 1995), Normalized Difference Water Index (NDWI) (Gao 1996), two-band EVI (EVI2) (Jiang et al. 2008), and Green-Red Vegetation Index (GRVI) (Motohka et al. 2010). Additional vegetation indices can be found in the agricultural drought section of part two of this review series (Chawla et al., 2020). In the past, the timeseries of vegetation indices have been used to monitor crop growth. Lunetta et al. (2010) used MODIS NDVI data to assess the cropping patterns in the Laurentian Great Lakes Basin. Skakun et al. (2017) used MODIS NDVI data along with air temperature information from MERRA2 reanalysis product to carry out winter crop mapping in Kansas (USA) and Ukraine. Tao et al. (2017) assessed spatio-temporal variations in the crop frequency using MODIS NDVI and EVI data along with ancillary information in Hubei province (China).

3.1.1.1. Crop yield estimation using vegetation indices.

In the case of crop yield estimation, the plethora of literature indicated the existence of the strong relationship between crop yield and vegetation indices (Anderson et al. 1993a; Shanahan et al. 2001; Tucker et al. 1980; Wiegand and Richardson 1990; Wylie et al. 1991). Several of these works established a regression relationship between vegetation index and observed crop yield and later used the relationship to predict crop yield with new vegetation index information. For instance, Bolton and Friedl (2013) setup linear regression between county-level yield and MODIS NDVI, EVI2, and NDWI in the Central United States. The crop yield information is obtained from data compiled by the United States Department of Agriculture (USDA) National Agricultural Statistics Service (NASS). Recently, Tuvdendorj et al. (2019) found that a combination of NDWI, NDVI, and visible and shortwave infrared drought index (VSDI) (Zhang et al. 2013) among nine considered vegetation indices performs best when linearly regressed with spring wheat yield.

Our review of the literature indicated that most of the works have aggregated the vegetation index over a period of time and then related

Table 1
List of satellites with optical/thermal sensors and their configurations. Note that the table is not exhaustive. We present only the sensors that are included as a part of this review.

Satellite	Sensor	Duration	Frequency Range (Number of Bands)	Spatial Resolution	Temporal Resolution
Landsat	Multispectral Scanner System (MSS)	1972 – present	500 nm – 1.1 µm (4 for Landsat 1,2,3, 4, and 5)	57 m, or 60 m	18 days, 16 days
	Thematic Mapper (TM) and Enhanced Thematic Mapper (ETM)	1972 – present	450 nm – 2.35 µm; 10.4 – 12.5 µm (7 for Landsat 4, and 5; 8 for Landsat 7)	30 m, 120 m	16 days
NIMBUS-7	Coastal Zone Color Scanner (CZCS)	1978 – 1995	433 nm – 12.5 µm (6)	825 m	6 days
Satellite pour l'Observation de la Terre (SPOT)	High Resolution Visible (HRV)	1986–2009	500 nm – 900 nm (4)	20 m	26 days
	High Resolution Visible and Infra-red (HRVIR)	1998 – 2013	500 nm – 1.75 µm (4)	20 m; 10 m	26 days
	Vegetation	1998 – 2015	430 nm – 1.75 µm (4)	1 km	26 days
IKONOS	Multispectral Sensor; Panchromatic Sensor	1999–2015	445 – 900 nm (5)	3.2 m, 0.82 m	3 days
Terra, Aqua	Moderate Resolution Imaging Spectroradiometer (MODIS)	2000 – present	400 nm – 14.4 µm (36)	250 m, 500 m, and 1 km	16 days
Earth Observatory-1	Hyperion	2000–2017	390 nm – 2.5 µm (2 2 0)	30 m	16 days
QuickBird	Multispectral Sensor; Panchromatic Sensor	2001–2015	450 – 900 nm	2.62 m, 0.65 m	1 – 3.5 days
ENVISAT	Medium Resolution Imaging Specrometer Instrument (MERIS)	2002 – 2012	390 – 1040 nm (15)	300 m; 1200 m	35 days
Meteosat Second Generation (MSG) geostationary satellites	Spinning Enhanced Visible and Infrared Imager (SEVIRI)	2004 – present	0.4 – 1.6 µm (4; visible/NIR); 3.9 – 13.4 µm (8 IR)	1 km; 3 km	–
METOP-A/B	Global Ozone Monitoring Experiment-2 (GOME-2)	2006 – present	240 – 790 nm (0.26–0.51 nm spectral resolution)	80 km × 40 km	1.5 days
WorldView-1/2/3/4	Panchromatic, multispectral, SWIR sensors	2007 – present	450–800 nm (panchromatic) 400–1040 nm (8; multispectral) 1195–2365 nm (8; SWIR)	0.31 m (panchromatic), 1.24 m (multispectral), 3.7 m (SWIR)	< 1 day
National Oceanic and Atmospheric Administration's (NOAA's) Polar Orbiting Environmental Satellites (POES)	Advanced Very High Resolution Radiometer (AVHRR)	2009 and 2012 – present	580 nm – 12.5 µm (6)	1.1 km; 4 km	1 day
NOAA-20	Visible Infrared Imaging Radiometer Suite (VIIRS)	2011-present	412 nm – 12.01 µm (22)	375 m, 750 m	16 days
Sentinel 2A and 2B	Multi-Spectral Imager (MSI)	2015 and 2017 – present	440 nm – 2.19 µm (12)	60 m, 20 m and 10 m	5 days
Greenhouse gases Observing SATellite (GOSAT)	Thermal And Near Infrared Sensor for carbon Observation - Fourier Transform Spectrometer (TANSO-FTS); Thermal And Near Infrared Sensor for carbon Observation - Cloud and Aerosol Imager (TANSO-CAI-2)	2018 – present	750 nm – 2.38 µm (4)	500, 1500 m	3 days

Table 2
List of satellites with active microwave sensors and their configurations. Note that the table is not exhaustive. We present only the sensors that are included as a part of this review.

Satellite	Sensor	Duration	Frequency Range (Number of Bands)	Spatial Resolution	Temporal Resolution
ENVISAT	Advanced Synthetic Aperture Radar (ASAR)	2002 – 2012	5.3 GHz (1)	30 m	35 days; 30 days (from 2010)
COSMO-SkyMed	SAR 2000	2007 - present	9.60 GHz (1)	1 m (SPOTLIGHT); 5 m (STRIPMAP-HIMAGE); 15 m (STRIPMAP-PINGPONG); 30 m (SCANSAR-WIDEREGION); 100 m (SCANSAR-HUGEREGION)	16 days
MetOp-A/B	Advanced SCATterometer (ASCAT)	2007 – present	5.225 GHz (1)	25 km	1–2 days
RADARSAT-2	Synthetic Aperture Radar (C-band)	2007 – present	5.405 GHz (1)	3–100 m	24 days
TerraSAR-X	SAR-X	2007 – present	9.65 GHz (1)	1.1 m (SPOTLIGHT); 3.3 m (STRIPMAP); 18.5 m (SCANSAR)	11 days
TanDEM-X	SAR-X	2010 – present	9.65 GHz (1)	1.1 m (SPOTLIGHT); 3.3 m (STRIPMAP); 18.5 m (SCANSAR)	11 days
RISAT-1	C Band Synthetic Aperture Radar (SAR)	2012–2017	5.35 GHz (1)	1 – 50 m	25 days
Sentinel 1A and 1B	C-band Synthetic Aperture Radar	2014 and 2016 – present	5.405 GHz	5 m × 5 m (stripmap mode), 5 m × 20 m (interferometric wide swath mode), and 25 m × 100 m (extra-wide swath mode); 5 m × 20 m (wave mode)	12 days

*indicates footprint

Table 3
List of satellites with passive microwave sensors and their configurations. Note that the table is not exhaustive. We present only the sensors that are included as a part of this review.

Satellite	Sensor	Duration	Frequency Range (Number of Bands)	Spatial Resolution	Temporal Resolution
Aqua	Advanced Microwave Scanning Radiometer-Earth Observing System (EOS) (AMSR-E)	2002–2011	6.925 GHz; 10.65 GHz; 18.7 GHz; 23.8 GHz; 36.5 GHz; 89.0 GHz (6)	56 km (6.925 GHz); 38 km (10.65 GHz); 21 km (18.7 GHz); 24 km (23.8 GHz); 12 km (36.5 GHz);5.4 km (89 GHz)	1–2 days
Microwave Imaging Radiometer using Aperture Synthesis (MIRAS)	Soil Moisture Ocean Salinity (SMOS) L-band radiometer	2010 – present	1.4 GHz (1)	< 50 km	2.5–3 days
GCOM-W	Advanced Microwave Scanning Radiometer 2 (AMSR2)	2012 – present	6.93 GHz; 7.3 GHz; 10.65 GHz; 18.7 GHz; 23.8 GHz; 36.5 GHz; 89 GHz	62 × 35 km (6.93 GHz); 62 × 35 km (7.3 GHz); 42 × 24 km (10.65 GHz); 22 × 14 km (18.7 GHz); 19 × 11 km (23.8 GHz); 12 × 7 km (36.5 GHz); 5 × 3 km (89 GHz)	1–2 days
Soil Moisture Active Passive (SMAP)	SMAP L-band radiometer	2015 – present	1.4 GHz (1)	47 × 39 km	1–3 days

Table 4
List of satellites that measure the gravity field and their configurations. Note that the table is not exhaustive. We present only the sensors that are included as a part of this review.

Satellite	Sensor	Duration	Frequency Range (Number of Bands)	Spatial Resolution	Temporal Resolution
Gravity Recovery and Climate Experiment (GRACE)	K-Band Ranging (KBR) twin-satellite system	2002 – 2017	24 GHz; 32 GHz	400 km	30 days
GRACE-Follow-On (FO)	K-Band Ranging (KBR) twin-satellite system	2018 – present	24 GHz; 32 GHz	400 km	30 days

to the corresponding crop yield instead of using instantaneous (satellite overpass) observations. This is because the nature of dependency between crop yield and spectral reflectance varies with crop growth (Labus et al. 2002; Rudorff and Batista 1990). Besides, temporal integration or aggregation of vegetation indices reduce the noise due to other factors (such as effects due to soils and clouds) in the vegetation responses. They also account for the total effect of photosynthesis (Benedetti and Rossini 1993; Rudorff and Batista 1990). The aggregation can be carried out by considering the maximum value of vegetation index, mean of peak values of vegetation index, the summation of vegetation index values in a crop cycle, vegetation index during the end of the season, among others. In this context, Funk and Budde (2009) indicated that NDVI accumulated during the mid-to-late season has a better correlation with the crop yield compared to other aggregation methods. Quarmby et al. (1993) used smoothened AVHRR (Advanced Very-High-Resolution Radiometer) NDVI integrated over the growing season for estimation of crop yield of wheat, cotton, rice, and maize crops through linear regression. Liu and Kogan (2002) used AVHRR Vegetation Condition Index (VCI) (Kogan, 1995) to monitor soybean crop production in Brazil. In this work, the authors considered the ratio of observed yield and trend yield (to account for technological improvements and an increase in food demand) as yield indicator. Lai et al. (2018) estimated wheat yield as a function of integrated Landsat NDVI (obtained during the growing season) with reasonable accuracy in the northern grain-growing region (NGR) of Australia. Mirasi et al. (2019) used the sum of Landsat 8 Operational Land Imager (OLI) NDVI values (during the growing period) as an indicator to estimate wheat yield in Iran. Their results indicated that the model simulates yield at the highest accuracy 49 days before harvesting during which wheat grains would turn milky matured.

Some studies also used a non-linear regression approach to estimate crop yield using vegetation index (Hayes and Decker 1996; Holzapfel et al. 2009; Ma et al. 2001; Mkhabela et al. 2011). Attempts have also been made to consider meteorological variables along with vegetation index as predictors in the statistical regression model to estimate the crop yield (Balaghi et al. 2008; Cai et al. 2019; Johnson 2014; Prasad et al. 2006; Shao et al. 2015).

3.1.1.2. LAI estimation using vegetation indices. Estimation of LAI using remote sensing techniques generally involved optical and microwave sensors. Early studies have used local-scale (field) measurements to linearly relate LAI with spectral reflectance information (Asrar et al. 1985; Gallo and Daughtry 1987; Gardner and Blad 1986). These works tested the applicability of NDVI and ratio vegetation indices (RVI; by considering various plausible wavelength combinations) (Pearson and Miller 1972). Johnson (2003) established linear regression between Ikonos NDVI and in-situ LAI in a Napa Valley vineyard. Fan et al. (2009) established linear and exponential relationships between NDVI and LAI using in-situ measurements over grasslands in Mongolia.

3.1.1.3. Use of hyperspectral vegetation indices. Despite the popularity of NDVI, the literature indicates that the NDVI values tend to saturate when the LAI values are very high (greater than 8) (Baret and Guyot 1991; Gu et al. 2013; Houborg et al. 2007; Wang et al. 2018). Gitelson (2004) attempted to reduce the effect of saturation by proposing a new index called the Wide Dynamic Range Vegetation Index (WDVI). Furthermore, hyperspectral vegetation indices have also exhibited an ability to reduce the saturation effect (Fang et al. 2019). The hyperspectral sensors also measure the reflectance from the red-edge vegetation spectrum – which is the sharp slope between low reflectance red spectrum and high reflectance NIR spectrum – situated between 350 and 1050 nm wavelength (Darvishzadeh et al. 2009; Thenkabail et al. 2000). Some of the vegetation indices that consider red-edge spectrum include Red-edge normalized difference vegetation index (NDVI-RE) (Gitelson and Merzlyak, 1994), Chlorophyll index Red-edge (CI-RE) (Gitelson et al., 2003), and Modified simple ratio Red-edge (R-RE) (Wu et al. 2008). Several studies have indicated a strong relationship between the red-edge inflection point (wavelength where the maximum slope of spectral reflectance is attained) and LAI of crops (Delegido et al. 2013; Dong et al. 2019; Gupta et al. 2003; Herrmann et al. 2011; Liu et al. 2004). Kira et al. (2016) ascertained that red-edge and NIR bands to be most informative for LAI estimation. Besides, several narrow-band vegetation indices are proposed that can accurately model the crop yield and LAI information (Haboudane et al. 2004; Thenkabail et al. 2000).

Attempts are made to compare the efficiency of multispectral and hyperspectral reflectances and associated vegetation indices towards the estimation of LAI and crop yield (Broge and Leblanc 2001; Lee et al. 2004; Mariotto et al. 2013; Thenkabail et al. 2002; Viña et al. 2011; Zhao et al. 2007). We find no consensus on which among the two sets of indices is more accurate. The accuracy of a vegetation index is found to be influenced primarily by the crop type, vegetation saturation, soil, and atmospheric effects, among others (Fang et al. 2019). Furthermore, sophisticated regression and machine learning techniques are also used to model crop yield and LAI using satellite sensor-based vegetation indices. Some of them include partial least square regression (Hansen and Schjoerring 2003; Li et al. 2014; Nguyen and Lee 2006), artificial neural networks (ANN) (Johnson et al. 2016; Panda et al. 2010), support vector machines (Durbha et al. 2007; Tuia et al. 2011), and random forests (Liang et al. 2015; Wang et al. 2016). Recently, Wang et al. (2018) estimated rice LAI using all of the above techniques and found random forests to perform better.

3.1.2. Physics-based methods

It is important to note that the above-described regression-based techniques are site-dependent and cannot be spatially transferrable. Due to this issue, these methods are only applicable at the local scale. Moreover, it is generally not possible to determine multiple variables through these techniques (Dorigo et al. 2007). Large scale simulation of crop biophysical variables requires the incorporation of the physics of the process into the modeling strategy. Land surface covered with vegetation will have reflectance from three components, 1) individual leaves, 2) canopy as a whole, and 3) soil type. Ideally, the physics-based models simulate reflectance from all the three components to estimate the top-of-canopy reflectance. The top-of-canopy reflectance values simulated from these models are then corrected for atmospheric effects – using an atmospheric radiative transfer model – to obtain top-of-atmosphere reflectance, which is comparable with measured satellite reflectance (Verhoef and Bach 2003; Vermote et al. 1997).

Leaf optical models and canopy reflectance models deal with simulating the scattering and absorption properties of leaves and canopy, respectively. One of the widely used leaf optical models is the PROSPECT model (Jacquemoud and Baret 1990), which is a radiative transfer model that simulates the optical properties of leaves in the wavelength range of 400–2500 nm. The PROSPECT model considers leaf mesophyll structure, pigment concentration, dry matter content, and water content as inputs. PROSAIL-4 and PROSAIL-5 models are the improved versions of the original model (Feret et al. 2008). Canopy reflectance models are categorized into kernel-based, turbid-medium, geometrical, and computer simulation models (Fang et al. 2019). Of these models, turbid-medium models are used widely. These models consider leaves as “small, randomly distributed absorbing and scattering elements with no physical size” (Dorigo et al. 2007). The Scattering by Arbitrarily Inclined Leaves (SAIL) model (Verhoef 1984) is a widely used canopy reflectance model. The SAIL model is a radiative transfer model, which considers primarily 1) canopy parameters (e.g., LAI and leaf angle distribution), 2) view and illumination parameters (e.g., view angle), 3) soil reflectance, and 4) leaf transmittance and reflectance parameters as inputs to simulate canopy bidirectional reflectance. The SAIL model, coupled with the PROSPECT model – in terms of providing leaf transmittance and reflectance – results in the PROSAIL model (Jacquemoud et al. 2009). Fig. 2 shows an illustration of the PROSAIL model (Berger et al. 2018).

Retrieval of crop parameters such as LAI through these physics-based models involves model inversion wherein the set of inputs that can minimize the error between simulated model atmosphere corrected reflectance and remotely sensed reflectance are estimated. Dorigo et al. (2007) noted three kinds of model inversion schemes, 1) model optimization, 2) lookup table approach (LUT), and 3) Artificial Neural Networks (ANNs). For instance, Bacour et al. (2006) used ANNs to train the synthetic data generated with the PROSAIL model and then retrieved LAI (along with other variables) using ENVISAT-MERIS reflectance information. Li et al. (2015) used multi-objective genetic algorithms based inversion of the PROSAIL model to retrieve LAI of winter wheat. Li et al. (2018) performed LUT inversion of the PROSAIL model to estimate LAI of winter wheat using China Centre for Resources Satellite Data and Application (CRESDA)’s GF-1 Wild Field Camera (WFV) data. Despite the applicability of physics-based models over larger areas, these models often suffer from the problem of equifinality, i.e., possibility of the existence of multiple solutions that result in optimality. Besides, model and observation uncertainties also result in the inversion to be an ill-posed problem. Several regularization schemes including incorporating prior information about variables of interest (for example, Combal et al. (2003)), have been proposed to circumvent the problem of equifinality in physics-based models (Atzberger 2004; Baret and Buis 2008; Rivera et al. 2013; Verrelst et al. 2013). Li et al. (2015) used the prior knowledge of the empirical relationship between LAI and leaf chlorophyll content (LCC) to improve the PROSAIL model inversion for the retrieval of winter wheat LAI.

Regression and physics-based models (radiative transfer model inversion) are used to obtain LAI products at global scales. Some of the operational products include MODIS MCD15A3H Version 6 (Myneni et al. 2015; Myneni et al. 2002), EUMETSAT’s SEVIRI (Spinning Enhanced Visible and Infra-red Imager) MSG (Meteosat Second Generation) LSA-423 (García-Haro et al. 2019), Visible Infrared Imaging Radiometer Suite (VIIRS) VNP15A2H (Myneni and Knyazikhin 2018; Yan et al. 2018), and AVHRR LAI Version 4 (Claverie et al. 2016) among others. Fang et al. (2019) provide a comprehensive list of global LAI products.

3.1.3. Assimilation of remote sensing data in crop simulation models

It can be noted that the physics-based models described above only consider the crop and soil-related parameters. Crop simulation models, on the other hand, consider the changing meteorological conditions, agricultural practices along with crop and soil conditions to simulate crop yield, among other variables. Some of the widely used crop simulation models include decision support system for agrotechnology transfer (DSSAT – a package of multiple crop models) (Hoogenboom et al. 2019; Jones et al. 2003), WOrld FOod Studies (WOFOST) (Boogaard et al. 1998; Van Diepen et al. 1989), Agricultural Production Systems sIMulator (APSIM) (Holzworth et al. 2014), Simulateur mulTIdisciplinaire pour les Cultures Standard (STICS) (Brisson et al. 2003), model for nitrogen and carbon dynamics in agro-ecosystems (MONICA) (Nendel et al. 2011), Daisy model (Abrahamsen and Hansen 2000), AquaCrop model (Raes et al. 2009; Steduto et al. 2009), Environmental Policy Integrated Climate Model (EPIC) (Williams et al. 1989), SWAP (Soil, Water, Atmosphere and Plant) model (Kroes et al. 2009), and Crop Environment REsource Synthesis – CERES (wheat – Godwin (1990); maize – Ritchie et al. (1989); barley – Otter-Nacke et al. (1991); rice – Singh et al. (1993)). Delécolle et al. (1992) noted three important characteristics of crop simulation models, 1) they can dynamically consider inputs at an interval and produce the outputs while updating the state variables, 2) they contain parameters, which can be tuned according to the growth period and the crop species, and 3) they take into account the crop development. Applying crop models over large areas can be challenging due to immense data requirements. Moreover, there can be uncertainties associated with the input datasets that affect the quality of the outcome. Remotely sensed information has the

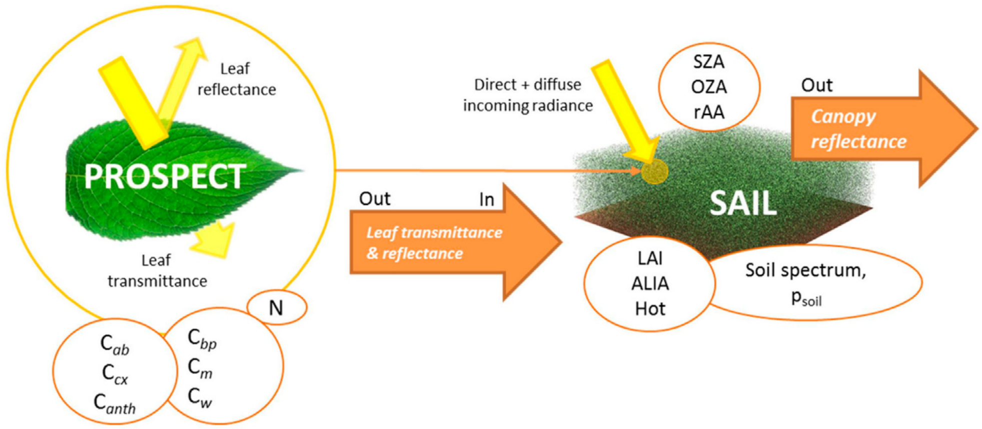

Fig. 2. Illustration of the PROSAIL model (reproduced from Berger et al. (2018)). Readers may refer to Berger et al. (2018) for details on the symbols used in the figure.

potential to address these issues. There are two ways of using remotely sensed crop growth variables in the crop simulation models, 1) replace them with model-simulated state variables to obtain output, and 2) use them to tweak the model state variables thereby altering the output. The second method is generally applied in a data assimilation framework.

3.1.3.1. Assimilation of vegetation variables. In the process of using remote sensing information, studies have used either the readily available products (discussed above) or used the state variables retrieved from the canopy reflectance model or regression-based model as an input to the crop simulation model. Some of the state variables, such as fPAR, LAI, canopy height, and above-ground biomass used in crop simulation models, can be "corrected" using remote sensing information (Dorigo et al. 2007). Doraiswamy et al. (2004) and Doraiswamy et al. (2005) used Landsat and MODIS reflectance respectively as input to the SAIL model (which is driven by in-situ measured leaf reflectance data) to retrieve LAI, which is fed as input along with weather and soil data to a simple climate-based crop model to obtain crop yield map. While Doraiswamy et al. (2004) used minimization of error between observed (in-situ) and simulated LAI to tune the SAIL model, Doraiswamy et al. (2005) also considered error between observed (satellite) and simulated reflectance in the objective function. A similar methodology is also implemented in other works (Migdall et al. 2009; Verhoef and Bach 2003).

It is important to note that by replacing the model simulated data with the satellite retrievals, the satellite-based output is assumed to be completely free from errors. In case, this assumption is violated, the quality of output from the crop models get affected. Data assimilation attempts to alleviate this issue by combining the satellite and simulated data by considering their error variance. So, the data assimilation scheme adjusts the state variable (e.g., LAI) simulated by the model based on satellite information. The modified state variable will alter the subsequent model fluxes (such as crop yield). Kalman filter (Kalman 1960), Ensemble Kalman Filter (Evensen 2003), Particle Filter (Arulampalam et al. 2002; Gordon et al. 1993), Variational Data Assimilation (Barker et al. 2004; Rawlins et al. 2007) are some of the widely used assimilation techniques. Liu et al. (2019) assimilated AMSR-E and SMOS soil moisture into the DSSAT model and found improvement in the accuracy of maize yield estimates in South Carolina, USA.

3.1.3.2. Assimilation of soil moisture. Apart from vegetation variables, the information on soil moisture plays an essential role in the aspects of agricultural management, monitoring droughts, and crop yield assessment, among others. Active and passive microwave remote sensing can be used to retrieve surface soil moisture content. It is important to note that the backscatter or the brightness temperature at top-of-canopy contains the contributions from canopy and soil (e.g., refer to WCM in Section 3.1.5.1). Therefore, having an accurate soil moisture information helps in separating these two contributions. Several retrieval algorithms are available to retrieve soil moisture from microwave observations (Karthikeyan et al. 2017; Wigneron et al. 2017). For instance, Ines et al. (2013) assimilated AMSR-E soil moisture and MODIS LAI in a modified DSSAT crop simulation model using EnKF to improve the yield estimation of maize crop. A similar attempt is made by Chakrabarti et al. (2014) in the context of SMOS to improve the estimates of soybean yield. Wit and Van Diepen (2007) assimilated ERS 1/2 scatterometer based soil moisture product into the WOFOST crop simulation model using EnKF to improve estimates of winter wheat crop yield. Soil moisture from passive microwave sensors is found to improve crop yield estimation (Mladenova et al. 2017). Recently, Huang et al. (2019) and Jin et al. (2018) provided a comprehensive review of data assimilation techniques used in the crop simulation models.

3.1.4. Crop yield assessment using remote sensing of plant photosynthetic activity

Photosynthetic activity influences biomass production (Hofius and Börnke, 2007). Therefore, Solar Induced Fluorescence (SIF) can be a direct indicator of crop yield, compared to the optical vegetation indices such as NDVI (which are responsive to only leaf area changes) (Guan et al. 2016; Guanter et al. 2014). SIF can be retrieved using physics-based radiative transfer models. For instance, the SAIL model is modified to include a fluorescence component (Miller et al. 2003; Rosema et al. 1991). The model proposed by Miller et al. (2003) is extended further to result in state-of-the-art Soil Canopy Observation, Photochemistry, and Energy fluxes (SCOPE) model (Tol et al. 2009). Pacheco-Labrador et al. (2019) used ground measurements as input to retrieve SIF, GPP, among other variables by inverting the SCOPE model. Recently, radiative transfer models with the ray-tracing technique are proposed to simulate fluorescence from a three-dimensional vegetation structure (suitable for crops) (Gastellu-Etchegorry et al. 2017; Zhao et al. 2016). The detailed developments on the remote sensing of SIF are presented by Meroni et al. (2009) and Mohammed et al. (2019).

Attempts are made to relate the remotely sensed SIF observations with GPP (Guanter et al. 2014; Hu et al. 2018; Liu et al. 2017). In one of the earlier studies, Guan et al. (2016) estimated GPP empirically over the USA using Global Ozone Monitoring Experiment–2 (GOME-2) based SIF data. Paul-Limoges et al. (2018) find that the type of diurnal relationship (linear or hyperbolic) between SIF and GPP is affected by the local environmental conditions. Somkuti et al. (2020) found a strong relationship between the Japanese Greenhouse gases Observing SATellite (GOSAT) based SIF retrievals and crop yields of corn and soybean in the USA. The satellite SIF data is used to estimate the crop yield using statistical regression (Cai et al. 2019; Guan et al. 2017). Attempts are now being made to couple the radiative transfer models that simulate SIF with biosphere models in an assimilation framework to improve the accuracy of GPP simulations (Norton et al. 2018).

3.1.5. Crop yield assessment using microwave data

Satellite microwave sensors measure the electromagnetic radiations emitted from the Earth's surface in the microwave spectrum. They can be classified into the active microwave (radar) and the passive microwave (radiometer) sensors. In the former case, the radar sends its beam of radiation towards the Earth's surface and measures the reflected signal in the form of backscatter coefficient (σ°). In the latter case, the radiometer measures the naturally emitted electromagnetic radiations from the Earth's surface in the form of brightness temperature (T_B). During this process, the microwave radiations get influenced by the dielectric properties of the target medium (e.g., vegetation, soil). Besides, these interactions are also influenced by the sensor configuration, such as polarization, incidence angle, and frequency. In contrast with the optical sensors, microwave radiations can penetrate through the clouds (essentially a transparent atmosphere, except during heavy rainfall) and are also independent of solar illumination. The following section presents the review of active and passive microwave remote sensing in crop monitoring applications.

3.1.5.1. Use of active microwave remote sensing. Active microwave (radar) remote sensing is used to retrieve crop variables, which include LAI, crop height, biomass, crop yield, and leaf structure. The radar backscatter measurements in higher frequencies (C and X bands) necessarily look at the upper layers of the canopy, which suits the retrieval of crop variables (Ulaby et al. 1984). L-band sensors, on the other hand, would have relatively greater penetration capability. So, the backscatter signal recorded by the sensors will have a significant effect due to soil, the effect of which needs to be separated to obtain accurate retrieval. Synthetic Aperture Radar (SAR) is used generally for crop monitoring applications (Steele-Dunne et al. 2017). Experiments have been carried out to assess the strength of relationship between backscatter coefficient and crop variables (Baghdadi et al. 2009; Bouman and van Kasteren 1990a,b; Brakke et al. 1981; Canisius et al. 2018; Chakraborty et al. 2005; Chen et al. 2009; De Loor et al. 1982; Fontanelli et al. 2013; Harfenmeister et al. 2019; Jiao et al. 2011; Lopez-Sanchez et al. 2010; Paloscia 1998). Kim and van Zyl (2009) proposed the Radar Vegetation Index (RVI), a function of backscatter coefficients in four polarizations (HH, VV, HV, VH) to estimate Vegetation Water Content (VWC) of rice and soybean. RVI is further used to monitor crop growth (Kim et al. 2011) and biomass (Wiseman et al. 2014). Furthermore, attempts are made to analyze the backscatter ratio (e.g. $\sigma^{\circ}_{HH}/\sigma^{\circ}_{VV}$) to assess their relationship with biomass (Satalino et al. 2009; Veloso et al. 2017), LAI (Chen et al. 2009), and crop growth (He et al. 2018).

Macelloni et al. (2001) attempted to relate multi-frequency SAR data (from airborne and satellite sensors) and biomass with a focus on broad and narrow leaf crops. They concluded that the backscattering increases with an increase in biomass in the case of broadleaf crops, and remains flat or decreases in the case of narrow-leaf crops. Some studies also reported saturation of backscatter at higher LAI or biomass (Asilo et al. 2019; Inoue et al. 2002; Jiao et al. 2011; Wiseman et al. 2014). Inoue et al. (2002) took multi-frequency (L, C, X, Ku, Ka bands), multiple incidence angles (20°-60°), and four polarizations (HH, VV, HV, VH) backscatter measurements over the complete growth of rice crop to compare with in-situ measured LAI, biomass, crop height, and stem density. Efforts also focused on understanding the influence of soil moisture and surface roughness on backscatter measurements while modeling crop variables (Major et al. 1994; Wang et al. 1987). Steele-Dunne et al. (2017) provided a comprehensive review of the developments that modeled crop variables using airborne and ground-based radars.

Retrieval of crop variables from radar backscatter measurements generally involve three kinds of models, 1) Water Cloud Model (WCM) (Attema and Ulaby 1978) – a semi-empirical model that assumes canopy as a cloud with uniform water droplets randomly distributed within the canopy, 2) energy and wave approaches – that involve physics of radiation interactions with vegetation, and 3) polarimetric decompositions – that extract elementary scattering contributions from the total backscatter. We find that WCM is widely used in the literature for modeling the crop variables. So, to keep the review concise, we limit the applications pertaining to only WCM. A detailed review of radar backscatter applications in agriculture can be obtained from Steele-Dunne et al. (2017). In WCM, the co-polarized backscatter coefficient (σ°_{pp}) from vegetation is computed as a summation of backscatter contribution from vegetation (σ°_{veg}), soil (σ°_{soil}), and their interactions (λ) (Eq. (1)).

$$\sigma^{\circ}_{pp} = \sigma^{\circ}_{veg} + \lambda^2\sigma^{\circ}_{soil} \tag{1}$$

where,

$$\sigma^{\circ}_{veg} = A \cdot V_1 \cdot \cos\theta \cdot (1 - \lambda^2) \tag{2}$$

$$\lambda^2 = \exp(-2 \cdot B \cdot V_2 \cdot \sec\theta) \tag{3}$$

$$\sigma^{\circ}_{soil} = C + D \cdot m_v \tag{4}$$

where, θ is the angle of incidence; A, B, C, and D are the empirical parameters, which need to be tuned according to the local conditions; V_1 and V_2 are the functions of vegetation indicators (here crop variables). So, WCM simulates σ°_{pp} as a function of the crop variable of interest and soil moisture along with four calibration parameters. Inoue et al. (2014) used C-band backscatter to establish a relationship with LAI and leaf biomass, and also retrieved LAI using WCM over rice fields in Japan. Hosseini et al. (2015) estimated LAI using WCM in corn and soybean with RADARSAT-2 (C-band) and Uninhabited Aerial Vehicle Synthetic Aperture Radar (UAVSAR) (L-band) data. Chauhan et al. (2019b) attempted to retrieve what crop height using RISAT-1 SAR data by coupling WCM with ANN. They considered a variable that includes plant height and other plant variables as vegetation indicators in WCM. Their study indicates that C-band backscatter is sensitive over corn and soybean, whereas L-band backscatter is sensitive over corn. We observed that WCM being used to retrieve crop variables and soil moisture (Hosseini et al. 2015) simultaneously as well as retrieve only crop variables with soil moisture obtained from ancillary sources (Bériaux et al. 2011).

It is important to note that inversion of WCM to determine crop variables is an ill-posed problem, which leads to equifinality, i.e., possibility of the existence of multiple combinations of vegetation variable and soil moisture that may result in an optimum value σ°_{pp}. Therefore, inverting WCM is a challenging task while retrieving the crop variables. Attempts are made to investigate several inversion techniques (e.g., optimization, LUT, SVR, and random forests) that address the ill-posed problem of WCM to retrieve crop variables using SAR data (Mandal et al. 2019a; Mandal et al. 2019b). Furthermore, Steele-Dunne et al. (2017) illustrated that the vegetation water content is not uniform along with the height of the canopy, and it also varies with the crop growth.

The models explained above are used primarily for the estimation of LAI and biomass, which are primary indicators of crop yield. In the case of retrieval of crop height – a strong indicator of crop phenology – radiative transfer models that describe the scattering nature of vegetation are available (Blaes et al. 2006; Bracaglia et al. 1995; Chuah et al. 1996; Karam et al. 1995; Karam et al. 1992; Le Vine et al. 1985; Ulaby et al. 1990; Wang et al. 2009; Yueh et al. 1992). They belong to the category of energy and wave approaches. These models consider canopy variables such as vegetation height, stem width, number of leaves, leaf angle, leaf size, dielectric constant, and backscatter from the soil as inputs to simulate the top-of-canopy backscatter. Although some attempts are made to retrieve crop height using these models (Le Toan et al. 1997; Zhang et al. 2014a,b), there may be a need to generate many datasets (e.g., using Monte Carlo simulations (Tsang et al. 1995)) to run the models (Erten et al. 2016).

SAR interferometry (InSAR) is another popular technique to retrieve vegetation height. The method is based on the phase difference between two spatially/temporally SAR acquisitions. However, this method has limited applications to retrieve crop height due to low spatial and temporal resolutions of satellite SAR sensors (Erten et al. 2016). Tandem interferometry – wherein two satellites are flown in close formation – circumvent these issues, and are useful in retrieving the crop height. The interferometric coherence (which measures the phase variance between two SAR images) and differential interferometric phase are key variables for crop height estimation in this method (Blaes and Defourny 2003; Rossi and Erten 2014). Studies have found a negative correlation between coherence and crop height (increase in crop height results in a decrease in coherence) (Engdahl et al. 2001; Srivastava et al. 2006). The TanDEM-X mission (Krieger et al. 2007), which contains twin X-band frequency satellites, became widely popular to retrieve crop height (Lee et al. 2018; Rossi and Erten 2014; Yoon et al. 2017).

Polarimetric Interferometric SAR (PolInSAR) is the advanced technology available to retrieve crop height information. This method uses polarimetry and interferometry to determine the three-dimensional structural parameters of vegetation (Cloude and Papathanassiou 1998). PolInSAR is used widely for estimating the forest height (Cloude et al. 2013; Garestier et al. 2007; Khati et al. 2017; Khati et al. 2018; Papathanassiou and Cloude 2001). The accuracy of height estimation is influenced by two important factors among others, 1) temporal decorrelation – degradation of phase quality that occurs due to structural and dielectric changes in the plant between two acquisitions, and 2) spatial baseline decorrelation – noise due to difference in positions of radar sensors between two SAR images that affect the scattering along the vertical coordinate (Zebker and Villasenor 1992). PolInSAR data is inverted to retrieve crop height typically using Volume-over-Ground (VoG) models. These models describe a volume of discrete scatterers (here crop canopy) on top of an impenetrable topography (here soil) (Pichierri and Hajnsek 2017).

There are two types of VoG models, 1) random-volume-over-ground (RVoG) model (Papathanassiou and Cloude 2001; Treuhaft and Siqueira 2000), and 2) oriented-volume-over-ground (OVoG) model (Treuhaft and Cloude 1999; Treuhaft and Siqueira 2000). After initial tests using airborne sensor and laboratory data (Lopez-Sanchez et al. 2007; Lopez-Sanchez et al. 2011), Lopez-Sanchez et al. (2017) proposed a methodology using VoG algorithms to retrieve rice crop height using TanDEM-X data. Erten et al. (2016) compared the backscatter radiative transfer model, PolInSAR, and InSAR based inversion algorithms for rice crop height estimation using TanDEM-X data. They recommended that an algorithm that combines the former two techniques can make more reliable crop height retrievals. Apart from InSAR and PolInSAR, crop height estimation is also possible with the polarimetric synthetic aperture radar (PolSAR) measurements. However, we find only limited applications involving PolSAR for the retrieval of crop height (Yuzugullu et al. 2016).

3.1.5.2. Use of passive microwave remote sensing. Passive microwave remote sensors (called radiometers) measures the naturally emitted electromagnetic radiations from the Earth's surface in the form of brightness temperature (T_B). Typically, the retrieval algorithm for vegetation involves a radiative transfer model (RTM). The RTM, when applied over low frequency (in L-, C-, and X- bands) measurements, can simulate the measured satellite T_B as a function of the Vegetation Optical Depth (VOD), a vegetation indicator that quantifies the total water content in the leaf and woody components of above-ground biomass (Liu et al. 2011). The VOD is found to have a relationship with optical vegetation indices (Grant et al. 2016; Lawrence et al. 2014; O'Neill et al. 2018), and radar backscatter measurements (Rötzer et al. 2017). In addition to the VOD, microwave vegetation indices (which are functions of dual-polarized T_B are also found to be useful to monitor vegetation (Becker and Choudhury 1988; Choudhury and Tucker 1987; Choudhury et al. 1987; Paloscia and Pampaloni 1992; Shi et al. 2008). Current retrieval algorithms can retrieve VOD using the satellite T_B measurements potentially without the need for ancillary vegetation information (Du et al. 2016; Fernandez-Moran et al. 2017; Jones et al. 2011; Karthikeyan et al. 2019; Konings et al. 2017; Konings et al. 2016; Owe et al. 2001).

VOD is reported as a potential indicator for crop yield estimation (Chaparro et al. 2018; Mladenova et al. 2017; Piles et al. 2017). VOD provides complementary information compared to optical indices such as EVI while estimating crop yield, given its ability to provide three-dimensional vegetation water content (Guan et al. 2016; Piles et al. 2017). VOD (from SMOS) is found to explain the crop growth and yield variability of corn (Hornbuckle et al. 2016; Patton and Hornbuckle 2012). Recently, Chaparro et al. (2018) proposed SMAP VOD seasonal metrics to assess crop yield variability over the north-central United States. On the other hand, Mladenova et al. (2017) observed low sensitivity of AMSR-E (Aqua satellite) VOD compared to MODIS NDVI and EVI while estimating crop yield over the central and eastern US. Attempts are being made to utilize the respective advantages of optical and passive microwave data synergistically to monitor crop yields (Mateo-Sanchis et al. 2019). Recognizing the importance of VOD, long term VOD products are being developed (Liu et al. 2011; Moesinger et al. 2019).

It is important to note that the satellite T_B measurements have a coarse spatial resolution (which is directly related to the frequency of the sensor) in the order of tens of kilometers. So, the agricultural studies using these measurements can be carried out with reasonable accuracy only when there is homogeneous agriculture taking place in the whole of the pixel. Besides, standing water, in the case of rice crops, can also impact the VOD retrievals (Piles et al. 2017).

3.2. Irrigation

Irrigation is defined as the full or partial application of water by artificial means (either surface or groundwater resources) to counter the precipitation deficit during the crop growth periods (Ozdogan et al. 2010). Irrigation is the largest consumer of freshwater resources, with the usage of approximately 70% of the groundwater withdrawals (Bastiaanssen et al. 2000). The irrigate water is sourced either from the surface (diverted from control structures such as dams) or groundwater resources.

Satellite remote sensing offers means to monitor irrigation at large scales. While we monitor irrigation, we primarily study three aspects a) identify the locations where irrigations would have taken place, and b) quantify either the amount of irrigation water supplied or the amount of water needed to reduce the crop water stress. This section deals with the developments concerning these perspectives of irrigation.

3.2.1. Mapping of irrigated areas

Accurate mapping of irrigated areas is necessary for a) achieving precise water allocations to agriculture, b) improving our understanding of water budget, and c) for the betterment of simulations from crop and hydrological models. If we consider optical satellite sensors, the information from MODIS, AVHRR, and Landsat is used widely for detecting the irrigation. We find irrigation mapping is carried out in two ways, 1) analyzing the spectral patterns of a single image to classify irrigated and non-irrigated areas, and 2) using images over a time period (e.g., crop growth period) to assess the spatio-temporal variations of irrigation patterns. The core concept of these two methods depends on the variations offered by irrigated areas in terms of spectral reflectance compared to other land cover categories.

3.2.1.1. Use of optical and infrared sensors. Traditionally visual interpretation is carried out to identify the irrigated regions using static maps (Heller and Johnson 1979; Rundquist et al. 1989; Thiruvengadachari 1981). The information from red and NIR bands is used widely for visual interpretation. These works also considered multiple images within a growing season to account for differences in the irrigation timing and growth stages. Despite its accuracy, visual interpretation is a cost and time-intensive process (Ozdogan et al. 2010). Also, the visual interpretation can be carried out only on a local scale. Image classification techniques tend to alleviate this problem. Some of the commonly used classification algorithms for this purpose include maximum likelihood technique, image segmentation technique, spectral matching technique, decision tree classification, density slicing with thresholds, and multi-stage classification (Abou EL-Magd & Tanton, 2003; Eckhardt et al. 1990; Manavalan et al. 1995; Simonneaux et al. 2008; Velpuri et al. 2009). Apart from spectral signatures, vegetation indices are also useful for irrigation mapping. NDVI is used widely for this purpose, given its ability to exhibit a considerable difference between irrigated and non-irrigated pixels (Ozdogan et al. 2006; Toomanian et al. 2004).

Several studies used multi-temporal images during crop growing season over several years for irrigation mapping. The multi-temporal analysis can consider the varying cropping patterns, planting dates, and crop growth, along with the extent of irrigation. In this context, Thenkabail et al. (2005) developed a comprehensive algorithm based on timeseries of MODIS spectral bands (2, 3, 5, 6, and 7) data to detect irrigation and rainfed classes along with crop onset, peak, and senescence (aging of the plant). The time series of spectral signatures are generally transformed into vegetation indices and are subjected to unsupervised classification or thresholding (value that differentiates irrigated and non-irrigated areas) to map the irrigation locations (Gumma et al. 2011; Jeong et al. 2012; Nhamo et al. 2019; Xiang et al. 2019; Xiao et al. 2005). For instance, Gumma et al. (2011) used eight-day composites of MODIS NDVI (circa 2001) to map irrigated areas with an unsupervised classification based framework in the Krishna basin, India. Xiao et al. (2005) combined eight-day composites of MODIS NDVI, EVI, and LSWI (Land Surface Water Index) using thresholding to detect flooded paddy fields of southern China. Xiang et al. (2019) attempted to differentiate the irrigated areas from forest pixels using a similar thresholding process involving MODIS NDVI and LSWI in northeastern China.

Efforts are made to use multi-temporal spectral information in a supervised classification framework (e.g., spectral matching techniques). Based on these techniques, the satellite information is correlated with the spectral bank (obtained from the ground), and the class that achieves maximum correlation (with satellite data at a location) will be assigned (Dheeravath et al. 2010; Thenkabail et al. 2007). Sharma et al. (2018) used Landsat NDVI, NDMI (Normalized Difference Moisture Index), and EVI timeseries from 1990 to 2015 in a supervised SVM (Support Vector Machine) classification framework to identify the irrigated areas in an Indian watershed with spatially heterogenous cropping system. It is important to note that the supervised analysis requires an adequate amount of ground-truth information in order to train the model. Uncertainties in the training data can affect the accuracy of classification. Furthermore, it is difficult to conduct supervised classification at continental scales. Some studies attempted to circumvent the requirement of ground data by using the Landsat reflectance information as a reference (Peña-Arancibia et al. 2014).

Irrigation can result in different crop growth patterns compared to that of exclusively rainfed agriculture (Thenkabail et al. 2005). Irrigated agriculture can result in 2.7 times more crop yield compared to rain-fed agriculture. Given these reasons, NDVI is predominantly higher in irrigated locations (increased greenness due to higher soil moisture). Hence, several studies utilized maximum NDVI composites for mapping irrigated regions (Biggs et al. 2006; Chance et al. 2018; Jin et al. 2016). For instance, Biggs et al. (2006) applied unsupervised classification over MODIS monthly maximum NDVI composite images for the year 2002 to detect irrigation areas in the Krishna basin, India. Jin et al. (2016) applied the Support Vector Machine (SVM) classification algorithm on HuanJing (HJ)-1A/B maximum NDVI timeseries to differentiate irrigated and rainfed wheat agriculture in China for circa 2011. Attempts are made to use peak NDVI information in thresholding based decision-tree algorithm framework to derive irrigated areas (Ambika et al. 2016; Pervez et al. 2014). Studies have reported similarity in the greenness of irrigated and rain-fed crops in humid regions (Ozdogan et al. 2010; Xiao et al. 2005). So, the inclusion of climate information in the classification algorithms can address the uncertainties (Kamthonkiat et al. 2005). Ozdogan and Gutman (2008) implemented decision trees classification algorithm to identify irrigated areas using MODIS NDVI and GI (Greenness Index) (Gitelson et al., 2005) along with climate and agricultural extent information over the CONUS region for circa 2001.

Chen et al. (2018) determined the irrigation attributes (extent, timing, and frequency) using MODIS and Landsat timeseries along with precipitation data, among others, in a heterogeneous landscape in northwestern China. Recently, Deines et al. (2019) developed high resolution (30 m) annual irrigation maps spanning from 1984 to 2017 over the central US. They used Landsat imagery and Google Earth Engine along with temperature, rainfall, soil, and terrain information as covariates in a random forest classifier along with other steps to produce the dataset.

3.2.1.2. Use of microwave sensors. In addition to optical sensors, satellite soil moisture products from microwave sensors are also used to identify the irrigated areas. Microwave sensors offer an advantage over optical sensors to provide measurements independent of solar illumination and cloud cover conditions. The operational soil moisture missions SMOS and SMAP achieved substantial improvements in terms of the accuracy of satellite soil moisture products. Lawston et al. (2017) found SMAP 9 km soil moisture products to have an ability to identify the spatio-temporal patterns of irrigation in the US. There have been attempts to compare the satellite soil moisture products with rainfall as well as vegetation patterns to assess the irrigated areas (Qiu et al. 2016; Singh et al. 2016). Notwithstanding the recent efforts, several hydrological models do not consider the effects of irrigation because of the challenges involved in coupling irrigation modules into the land surface model schemes. In this regard, attempts are made to compare soil moisture simulations from these models (that do not consider irrigation effects) with satellite soil moisture products (which consider both rainfall and irrigation effects on soil moisture) in order to identify the irrigated areas (Escorihuela and Quintana-Seguí 2016; Kumar et al. 2015; Malbeteau et al. 2018; Zhang et al. 2018).

Research is also conducted to assess the potency of radar backscatter measurements to detect irrigated areas. Fieuzal et al. (2011) found that σ°_{HH} Envisat/ASAR sensor is sensitive to irrigated areas in the wheat-growing seasons in Yaqui irrigated area, Mexico. Similarly, Hajj et al. (2014) found that the timeseries of TerraSAR-X and COSMO-SkyMed X-Band SAR backscatter is sensitive to the irrigation events over grasslands. Recently, attempts are made to use backscatter measurements in a classification framework to derive irrigation map (Bazzi et al. 2019; Bousbih et al. 2018; Gao et al. 2018; Sharma et al. 2019). For instance, Bazzi et al. (2019) used Sentinel 1 SAR timeseries in three classification algorithms – wavelet-random forest, principle component analysis-random forest, and convolution neural network (CNN) classifiers – to map irrigated and non-irrigated areas in Catalonia, Spain.

3.2.1.3. Global products of irrigated area. Few attempts are made to map the irrigated areas (or areas indicative of irrigation) at the global scale.

The Global Map of Irrigated Areas version 5 (GMIA 5.0) product spanning from 2000 to 2008 (Siebert et al. 2015), and MIRCA2000 product for circa 2000 (Portmann et al. 2010) are the two datasets prepared used the census information. These two products are available at 5 arc-minute resolution. Global irrigated area map (GIAM) is a global product developed using meteorological data, land use, and multiple satellite sensors information (Thenkabail et al. 2009b). The product primarily uses unsupervised classification and is available at 1 km resolution for circa 2000. The Global Rain-fed, Irrigated, and Paddy Croplands (GRIPC) map is another global product that is based on statistics, climate, and satellite sensor data (Salmon et al. 2015). This product is developed using a decision-tree algorithm at a 500 m resolution for the year 2005. The ESA under Climate Change Initiative (CCI) produced a global land cover map, containing irrigated and non-irrigated areas, at 300 m resolution for the years 2000, 2005, and 2011 using Medium Resolution Imaging Spectrometer (MERIS) data with unsupervised clustering and expert knowledge (Bontemps et al. 2013). Meier et al. (2018) developed a 1 km resolution global irrigated area product spanning from 1999 to 2012. The product is based on GMIA and satellite/reanalysis/observations based vegetation, agriculture, land cover, and precipitation information. Recently, Zohaib et al. (2019) developed global irrigated areas product for the year 2015 using satellite-based soil moisture, LST, and surface albedo along with reanalysis products. It is important to note that these datasets are difficult to validate at the global scale due to the lack of observed data. Studies also noticed discrepancies when these products are evaluated at local scales (Meier et al. 2018; Thenkabail et al. 2009a; Thenkabail et al. 2009b).

3.2.2. Quantification of irrigation water

Unlike identifying the irrigated areas, it is challenging to quantify the irrigation water at large scales. This is because, 1) the observed information of the volume of irrigated is limited to limited spatio-temporal scales, 2) technical and legal constraints of setting up in-situ stations (Brocca et al. 2018). Besides, the heterogeneous agricultural system with varying irrigation practices can lead to significant uncertainties in the irrigation estimates. In literature, we find two ways in which the irrigation water is quantified, 1) estimate Irrigation Water Requirement (IWR), and 2) estimate Irrigation Water Consumption (IWU). According to the definitions provided by Allen et al. (1998), the IWR is the difference between the Crop Water Requirement (CWR) and effective precipitation. It is the amount of water that should be supplied to maintain the potential transpiration of the crop (Calera et al. 2017). The IWR also considers water needed for leaching of salts and compensates for the non-uniform water application. Apart from ET_{crop}, IWR is a function of precipitation, soil moisture, and soil properties. The CWR is the amount of water required to manage the losses due to crop evapotranspiration (ET_{crop}). Several works used these schemes as basis to model the IWR (Döll and Siebert 2002; Hanasaki et al. 2010; Hanasaki et al. 2006; Pokhrel et al. 2012; Rost et al. 2008; Siebert et al. 2010; Sulser et al. 2010; Van Dijk et al. 2018; Wada et al. 2011; Wisser et al. 2008).

3.2.2.1. Estimation of irrigation water requirement (IWR). ET_{crop} is one of the important variables to estimate IWR. ET_{crop} is influenced by climate (air temperature, humidity, radiation, and wind speed) and crop (growth stage, crop height, and rooting characteristics, etc.) conditions (Allen et al. 1998). Traditionally Penman-Monteith (PM) equation is used to estimate ET_{crop} for determining the CWR. This equation is derived from surface energy balance and aerodynamic resistance equations. The PM equation, under standard conditions of vegetation, as defined by the Food and Agriculture Organization (FAO), can be used to determine reference crop evapotranspiration (ET_0) (Allen et al. 1998). ET_0 multiplied with crop coefficient (k_c) yields ET_{crop}. k_c is dependent on crop characteristics and soil evaporation conditions. k_c can be determined using remote sensing products through its relationship with vegetation indices such as NDVI and SAVI (Calera et al. 2017). Remote sensing information can be used to estimate directly ET_{crop} using surface energy balance methods. ET is estimated through latent heat flux (product of latent heat of vaporization and ET) in the energy balance equation. The two-source energy balance (TSEB) (Norman et al. 1995), the surface energy balance algorithm (SEBAL) (Bastiaanssen et al. 1998), the simplified surface energy balance index (S-SEBI) (Roerink et al. 2000), and the surface energy balance system (SEBS) (Su 2002) are some of the widely used energy balance models to estimate ET. Attempts are made to compare these models for their accuracy (Eswar et al. 2017; Wagle et al. 2017). Apart from IWR, irrigation scheduling is also necessary to prevent crops from water stress. The remotely sensed Crop Water Stress Index (CWSI) (Jackson et al. 1981), computed as a function of the differences between canopy and air temperatures, is widely used for this purpose (Gontia and Tiwari 2008; O'Shaughnessy et al. 2012; Veysi et al. 2017). Attempts are also made to assess the efficiency of irrigation by considering vegetation indicators and water policies along with ET_{crop} (Al Zayed and Elagib 2017). Further information on crop and irrigation water requirements can be obtained from Calera et al. (2017).

3.2.2.2. Estimation of irrigation water use (IWU). In the case of IWR, the irrigation withdrawals from the source are estimated, which may or may not be translated to actual irrigation usage due to either under or over-irrigation. Besides, the uncertainty in ET can also impact the accuracy of IWR estimates. Analyzing the soil moisture variations concerning precipitation can indicate the amount of water consumed through irrigation (IWU). Recent efforts have focused on using this concept to determine the IWU. (Brocca et al. 2014; Brocca et al. 2013) have developed precipitation datasets using soil moisture as the driving variable. The underlying algorithm called 'SM2RAIN' is applied to several soil moisture products (Brocca et al. 2016; Ciabatta et al. 2017). The IWU is attributed to the systematic differences between the resultant precipitation from SM2RAIN and the actual precipitation data (Brocca et al. 2018; Jalilvand et al. 2019). In a similar attempt, Zaussinger et al. (2019) quantified IWU by determining the systematic difference between the satellite soil moisture products (SMAP, AMSR2, and ASCAT) and reanalysis soil moisture product (MERRA-2, which does not account for irrigation) over the Contiguous United States (CONUS) region. Besides, attempts are being made to arrive at IWU by estimating the difference between the soil moisture simulations from land surface model simulations (that do not consider irrigation effects) and the soil moisture simulations obtained by assimilating satellite soil moisture into the land surface model (to account for the irrigation effects) (Abolafia-Rosenzweig et al., 2019; Nair and Indu 2019). It may be noted that the satellite products provide soil moisture of only surface (~5 cm) (Karthikeyan et el., 2017). However, the uptake of water from soil depends on the root depth of the crop species. Therefore, it is important to quantify the rootzone soil moisture to infer accurately about the IWU. In this regard, attempts are being made to simulate rootzone soil moisture by assimilating satellite soil moisture products in a land surface models using data assimilation algorithms (Das and Mohanty, 2006; De Lannoy and Reichle, 2016; Li et al., 2010; Liu and Mishra, 2017; Martens et al., 2017; Reichle et al., 2017; Reichle et al., 2019). Similar attempts are being made to assimilate Gravity Recovery and Climate Experiment (GRACE) Terrestrial Water Storage (TWS) in land surface models (Girotto et al., 2019; Tian et al., 2019).

3.3. Crop losses

Crop losses significantly affect agricultural productivity. They occur due to abiotic factors and biotic factors (Oerke 2006). The former include irradiation, water, temperature, and nutrients. The latter include pests, diseases, and weeds. Crop lodging (roots may lose the anchorage to sustain the crop) as a result of some of the abiotic factors. Satellite remote sensing is increasingly being used to detect crop losses. The detection is possible when there is a difference in the spectral signature from the crop, which is affected by any of the above-described factors. Some of the losses may not be detectable in case they do not exhibit differentiable spectral patterns.

3.3.1. Pests and diseases

Pests and diseases damage the crops primarily in four ways, 1) reduction of biomass due to destruction of leaf, stalk and stem, 2) development of crop lesions or pustules due to infections, 3) destruction of leaf pigments, and 4) wilting of plants (Zhang et al. 2019). Wheat rusts, locusts, armyworms, fruit flies, rice blast, sheath blight of rice, mildew, leafhopper, aphid bugs, beetles, and rhizomania are some of the crop pests and diseases, which can be detected through remote sensing. Efforts are being made to detect losses due to pests and diseases at the leaf, canopy, and regional scales. Satellite remote sensing in optical and NIR frequencies is used prominently at a regional scale for this purpose. Apart from optical and NIR satellite sensors, attempts are made to use fluorescence and microwave measurements for detecting pests and diseases. However, most of the studies are limited to the leaf/canopy scales. Information from both multispectral and hyperspectral satellite sensors – which include Landsat, MODIS, Hyperion, SPOT, among others – is found to be useful for pest and disease detection (Bauriegel et al. 2011; Eklundh et al. 2009; Oumar and Mutanga 2013; Pengra et al. 2007; Yuan et al. 2014). Apart from widely used vegetation indices such as NDVI, EVI, NDWI, and LAI, indices such as Disease Water Stress Index (DWSI) (Apan et al. 2004), Disease Index (DI) (Zheng et al. 2018) and Yellow Rust Index (YRI) (Huang et al. 2014) for detecting wheat yellow rust, Aphid Index (AI) (Luo et al. 2013), and Leafhopper Index (LHI) (Prabhakar et al. 2011), among others are proposed for pest and disease detection.

The growth of pests and diseases require suitable vegetation and meteorological conditions (Coops et al. 2006). The Tasseled Crop Transformation (TST) (Crist and Cicone 1984) – that determines parameters such as brightness, greenness, and wetness of vegetation – is generally used to identify the vegetation conditions that are prone to pests and diseases. The combined use of these datasets is found to improve the accuracy of the detection of pests and diseases (Bhattacharya and Chattopadhyay 2013; Yuan et al. 2017; Zhang et al. 2014a). It may be noted that a crop can be subjected to various forms of pests and diseases during its growth. Besides, there may be spatial heterogeneity of species of pests and diseases in the field. Hence it is essential to assess the spatio-temporal heterogeneities along the severity of pests and diseases to strategize their treatment. It is possible to identify these heterogeneities through the differences in the patterns of reflectance. This task can be achieved through the classification algorithms such as Artificial Neural Network (ANN), random forests (RF), partial least squares discriminant analysis (PLS-DA), maximum likelihood classifier, Bayesian classifiers, among others (da Rocha Miranda et al. 2020; Dhau et al. 2019; Yuan et al. 2014). In the case of hyperspectral remote sensing, spectral unmixing algorithms are used to discriminate pests and diseases (Fitzgerald et al. 2004; Franke and Menz 2007). On the other hand, the severity of pests and diseases can also be identified using machine learning regression-based algorithms (Chemura et al. 2017; Liu et al., 2019a,b; Oumar and Mutanga 2013). Satellite revisits are found to be useful to carry out multitemporal analysis to assess the spread of pests and diseases (Dhau et al. 2019; Eklundh et al. 2009; Franke and Menz 2007; Ji et al. 2004; Wulder et al. 2008; Zhang et al. 2016; Zhang et al. 2014b). Further details on the applications of remote sensing to detect crop pests and diseases can be obtained from (Zhang et al. 2019).

3.3.2. Crop lodging

Crop lodging is the displacement of stem or root anchorage from their vertical position (Pinthus 1974). It occurs mainly in cereal crops (rice, wheat, barley, etc.) (Chauhan et al.,2019a,b). Some of the factors that cause crop lodging include wind forces, rains, soil strength, plant population density, nitrogen nutrition, plant growth regulators, stem diseases, weak stems, and weak root anchorage (Kendall et al. 2017). Crop lodging has resulted in losses of £47-120 million for rapeseed crop (Kendall et al. 2017) and $80 million for winter wheat crop (Berry et al. 1998) in the UK per year. Crop lodging results in the reduction of crop height, crop inclination, and crop yield, which is dependent on the crop growth stage at which lodging would have occurred. Identifying these features through remote sensing information can be crucial to detect crop lodging. Although detection of crop lodging is widely carried out at field scale using in-situ and airborne remote sensors, the use of satellite remote sensing is still at primitive stages (Chauhan et al.,2019a,b). Besides, most of the studies use backscatter from active microwave satellite sensors for this purpose.

The studies that carried out a qualitative detection used radar backscatter coefficients or their ratios to identify lodging and non-lodging regions. In one of the first studies, (Yang et al. 2015) used backscatter polarization ratio, odd-scattering contribution ratio, and the double-bounce scattering ratio in total scattering obtained from RADARSAT-2 to detect wheat lodging regions. Similar attempts are carried out by Zhao et al. (2017) and Li et al. (2019) to detect wheat and canola and sugarcane lodging, respectively, using RADARSAT-2 data. Some studies used the reduction of crop height as an indicator to arrive at a quantitative assessment of crop lodging. Han et al. (2017) used crop height as a proxy to estimate the severity of corn lodging. Shu et al. (2019) estimated the lodging angle (crop inclination) by determining the crop height before and after lodging of maize crop using Sentinel-1 SAR data. Recently, Chauhan et al. (2020) modeled crop inclination (in-situ measurement) and polarization metrics derived from Sentinel-1 and RADARSAT-2 data using Support Vector Regression (SVR) technique. Further details on the status of remote sensing of crop lodging detection can be obtained from Chauhan et al. (2019).

3.3.3. Weeds

Weeds are competitive (or invasive) plants that grow in farms. They reduce crop productivity since they compete for the inorganic nutrients with crops (Oerke 2006). Weeds account for almost 34% of the global crop losses and can potentially lead to the highest crop losses compared to other factors (Oerke 2006). However, they can be destroyed either through mechanical treatment or by spraying herbicides. For the effective operation of these treatments, it is essential to identify the locations of weeds, which can be carried out using remote sensing. In the past, airborne sensors are used widely to identify the locations affected by weeds (Thorp and Tian 2004). Currently, Unmanned Aerial Vehicles (UAVs) are regularly being used for field-scale identification of weeds. Since satellite remote sensing retrieves information at the coarser spatial resolution, it can be challenging for weed detection given their size and patchiness (Müllerová et al. 2017).

Weeds can be identified from the difference in the spectral patterns of reflectivities compared to that of a crop. Initial studies used band reflectance information from satellites such as SPOT, Landsat TM, and AVHRR in classification algorithms to identify weed-infested regions (Anderson et al. 1993b; Everitt et al. 1993; Peters et al. 1992; Ullah 1989). Attempts are made to identify weeds using vegetation indices. (Backes and Jacobi 2006) used NDVI from QuickBird in a supervised classification framework to identify weed patches. Castillejo-González et al. (2014) used band reflectance and NDVI of Quickbird in seven classification algorithms to identify wild oat patches in wheat fields. Similar attempts are made using Sentinel-2A, Landsat 8, SPOT-5, and Worldview-2 data (Matongera et al. 2017; Odindi et al. 2014; Ottosen et al. 2019; Tarantino et al. 2019). We find the usage of satellite sensors for weed detection limited mostly to commercial satellites, which provide reflectance information at very high spatial resolution (< 10 m).

4. Summary

In this work, we review three aspects of the role of satellite remote sensing for managing agriculture, 1) crop growth and yield assessment, 2) irrigation mapping and quantification, and 3) crop losses. In this process, we reviewed how satellite sensors that measure signals from the Earth's surface across various frequencies, including optical, thermal, and microwave spectrum, are contributing to the above areas of research. Following is the summary of the review.

- **Crop growth and yield assessment:** Regression relationship with indices such as NDVI, RVI, and VCI are used to estimate crop yield and LAI. Both multispectral and hyperspectral imageries are found to be useful for this purpose. Physical models, such as the PROSAIL model (that simulates canopy reflectance as a function of LAI and other variables/parameters), are widely used to retrieve LAI. Besides, crop simulation models account for climate and agricultural conditions for simulating crop variables. Data assimilation has turned into a useful tool to synergistically combine model simulations and remote sensing data for improving the crop state variables such as fPAR and LAI. With increased efforts of obtaining soil moisture observations at global scales (using microwave sensors), attempts are made to ingest soil moisture (in data assimilation framework) into crop simulations models to improve the estimation of crop yield. SIF is one of the emerging areas of research. Attempts are made to use SIF measurements to determine GPP and crop yield through regression analysis. The radar microwave signals, due to their ability to penetrate through the atmosphere, are being used widely for crop growth assessment. These studies use methods such as semi-empirical models (e.g., WCM), energy and wave approaches, and polarimetric decomposition to retrieve crop variables such as LAI and biomass. Crop monitoring is also carried out by estimating crop height. For this purpose, InSAR, tandem interferometry, PolSAR, and PolInSAR techniques are widely used. Research is initiated to study the linkage between passive microwave VOD and crop growth in regions where agriculture is practiced in large spatial scales.
- **Irrigation:** Remote sensing information contributes to irrigation research by either identifying the irrigated areas or quantifying the amount of water required/supplied. Optical/thermal reflectance information collected over several years is subjected to either supervised or unsupervised classification algorithms to identify the irrigated areas. Derived products such as NDVI, NDMI, EVI, LSWI are also used in classification schemes for this purpose. Similar classification schemes are applied to backscatter timeseries from radar sensors for detecting irrigation. In the case of passive microwave sensors, the soil moisture obtained measures the moisture changes due to rainfall as well as irrigation events. Therefore, attempts are made to use soil moisture products to identify the spatial and temporal patterns of irrigated areas. ET is an essential variable for quantifying the irrigation water requirement. Energy balance methods are popular in determining ET using optical/thermal reflectance from satellites. On the other hand, the identification of irrigation water supplied to a farm is a primary function of soil moisture. Recent efforts have focused on extracting the irrigation information by using satellite soil moisture and precipitation datasets.
- **Crop losses:** Crop losses due to pests and diseases are detected at a large scale using optical/thermal reflectance data. Apart from vegetation indices, disease detection indices such as Aphid Index, DWSI, among others, are used. The spread of pests and diseases are identified by applying classification algorithms on multi-temporal data. However, such detection is possible only when the reflectance from pest/disease affected plant exhibit significantly different spectral pattern compared to that of a healthy leaf. Although efforts are being made to use microwave or SIF data for pests and disease detection, the experiments are confined, as of now, to field scale (using field/airborne sensors). Crop lodging is another cause of crop losses. Currently, crop lodging is detected using backscatter measurements. Since lodging is linked with crop height, the detection algorithms derive height and its related parameters (such as inclination). Lastly, weeds, which lead to crop losses, are detected using vegetation indices and classification algorithms.

5. Outlook

The following conclusions can be drawn from this review.

- There is a need to develop robust algorithms that determine the crop productivity (in terms of yield) in heterogeneous agricultural systems since most of the research focused on scales that match satellite footprint. Upcoming satellite missions such as NASA-ISRO SAR mission (NISAR) (https://nisar.jpl.nasa.gov/), which can retrieve backscatter as high as 10 m spatial resolution, can contribute to addressing the need. Besides, planned missions such as Copernicus Microwave Imaging Radiometer (CMIR) (Kilic et al., 2018) based on multi-frequency (L, C, X, Ka/Ku) bands brightness temperature measurements can contribute towards obtaining enhanced operational products.
- There are challenges associated with application of crop models in terms of parameter calibration, large scale applicability, and quantification of uncertainties. Although data assimilation is intended to complement with some of these issues, most of the research is focused on assimilating only LAI. There is a need to carry out multivariable assimilation to improve the quality of crop yield simulations. In this process, the issues pertaining to the mismatch between spatio-temporal scales of different sensors, as well as crop models, need to be addressed.
- Over the recent years, satellite sensor based Solar Induced Fluorescence (SIF) is gaining much importance due to its ability to capture the plant's photosynthetic activity. There is a need to develop crop models that can simulate plant fluorescence so that SIF from satellites can be ingested to improve the yield estimation. ESA's future mission Fluorescence Explorer (FLEX) (Drusch et al., 2017) dedicated to measure SIF shall contribute towards these research efforts.
- Uncertainties persist in the irrigation assessment in terms of quantifying both requirements and utilization through satellite remote sensing. Addressing this challenge requires in-situ information of irrigation water supplied to farms.
- Detecting irrigation under heterogeneous agriculture with varying irrigation scheduling at the plot scale remains a concern. For this purpose, the possibility of integrating remote sensing data with hydro-economic models (Harou et al. 2009) (that take into account water allocation policy, water pricing, among others) can be explored.
- It is challenging to detect pests and diseases in the early stages since most of them originate from the base of the plant. The crop would have been already destroyed by the time leaves get affected (which could be detected with remote sensing). Multi-look angle sensors may aid in early detection of pests and droughts.
- A crop may be subjected to variety of stresses, which change over its growth cycle. Efforts have to be made to differentiate the stresses using satellite sensors so as to precisely strategize the crop protection.
- Most of the research on crop losses is currently being carried out using Unmanned Aerial Vehicles (UAVs), which have very high resolution. There is a need to develop a framework of integrating information from UAVs at a local scale with satellite sensors, which have a global reach for large scale monitoring of crop losses in realtime.

CRediT authorship contribution statement

L. Karthikeyan: Conceptualization, Formal analysis, Investigation, Writing - original draft. **Ila Chawla:** Conceptualization, Formal analysis, Investigation, Writing - original draft. **Ashok K. Mishra:** Conceptualization, Formal analysis, Supervision, Writing - review & editing, Funding acquisition.

Declaration of Competing Interest

The authors declare that they have no known competing financial interests or personal relationships that could have appeared to influence the work reported in this paper.

Acknowledgments

This study was supported by the National Science Foundation (NSF, USA) award # 1653841 and 1841629. Authors acknowledge Abhishek Kumar, Azad Patle and Sumant Tyagi (Masters students of CSRE, IIT Bombay) for their assistance in compiling the literature.

References

Abolafia-Rosenzweig, R., Livneh, B., Small, E., Kumar, S., 2019. Soil moisture data assimilation to estimate irrigation water use. J. Adv. Model. Earth Syst.
Abou EL-Magd, I., Tanton, T., 2003. Improvements in land use mapping for irrigated agriculture from satellite sensor data using a multi-stage maximum likelihood classification. Int. J. Remote Sens. 24, 4197–4206.
Abrahamsen, P., Hansen, S., 2000. Daisy: an open soil-crop-atmosphere system model. Environ. Modell. Software 15, 313–330.
Al Zayed, I.S., Elagib, N.A., 2017. Implications of non-sustainable agricultural water policies for the water-food nexus in large-scale irrigation systems: A remote sensing approach. Adv. Water Resour. 110, 408–422.
Allen, R.G., Pereira, L.S., Raes, D., Smith, M., 1998. Crop evapotranspiration-Guidelines for computing crop water requirements-FAO Irrigation and drainage paper 56. Fao, Rome 300, D05109.
Ambika, A.K., Wardlow, B., Mishra, V., 2016. Remotely sensed high resolution irrigated area mapping in India for 2000 to 2015. Sci. Data 3, 160118.
Anderson, G., Hanson, J., Haas, R., 1993a. Evaluating Landsat Thematic Mapper derived vegetation indices for estimating above-ground biomass on semiarid rangelands. Remote Sens. Environ. 45, 165–175.
Anderson, G.L., Everitt, J.H., Richardson, A.J., Escobar, D.E., 1993b. Using satellite data to map false broomweed (Ericameria austrotexana) infestations on south Texas rangelands. Weed Technol. 7, 865–871.
Apan, A., Held, A., Phinn, S., Markley, J., 2004. Detecting sugarcane 'orange rust'disease using EO-1 Hyperion hyperspectral imagery. Int. J. Remote Sens. 25, 489–498.
Arulampalam, M.S., Maskell, S., Gordon, N., Clapp, T., 2002. A tutorial on particle filters for online nonlinear/non-Gaussian Bayesian tracking. IEEE Trans. Signal Process. 50, 174–188.
Asilo, S., Nelson, A., de Bie, K., Skidmore, A., Laborte, A., Maunahan, A., Quilang, E.J.P., 2019. Relating X-band SAR Backscattering to Leaf Area Index of Rice in Different Phenological Phases. Remote Sensing 11, 1462.
Asrar, G., Kanemasu, E.T., Yoshida, M., 1985. Estimates of leaf area index from spectral reflectance of wheat under different cultural practices and solar angle. Remote Sens. Environ. 17, 1–11.
Attema, E., Ulaby, F.T., 1978. Vegetation modeled as a water cloud. Radio Sci. 13, 357–364.
Atzberger, C., 2004. Object-based retrieval of biophysical canopy variables using artificial neural nets and radiative transfer models. Remote Sens. Environ. 93, 53–67.
Backes, M., Jacobi, J., 2006. Classification of weed patches in Quickbird images: verification by ground truth data. EARSeL eProceedings 5, 173–179.
Bacour, C., Baret, F., Béal, D., Weiss, M., Pavageau, K., 2006. Neural network estimation of LAI, fAPAR, fCover and LAI× Cab, from top of canopy MERIS reflectance data: Principles and validation. Remote Sens. Environ. 105, 313–325.
Baghdadi, N., Boyer, N., Todoroff, P., El Hajj, M., Bégué, A., 2009. Potential of SAR sensors TerraSAR-X, ASAR/ENVISAT and PALSAR/ALOS for monitoring sugarcane crops on Reunion Island. Remote Sens. Environ. 113, 1724–1738.
Balaghi, R., Tychon, B., Eerens, H., Jlibene, M., 2008. Empirical regression models using NDVI, rainfall and temperature data for the early prediction of wheat grain yields in Morocco. Int. J. Appl. Earth Obs. Geoinf. 10, 438–452.
Baret, F., Buis, S., 2008. Estimating canopy characteristics from remote sensing observations: Review of methods and associated problems. *Advances in land remote Sensing*. Springer, pp. 173–201.
Baret, F., Guyot, G., 1991. Potentials and limits of vegetation indices for LAI and APAR assessment. Remote Sens. Environ. 35, 161–173.
Barker, D.M., Huang, W., Guo, Y.-R., Bourgeois, A., Xiao, Q., 2004. A three-dimensional variational data assimilation system for MM5: Implementation and initial results. Mon. Weather Rev. 132, 897–914.
Bartlett, D., Hardisky, M., Johnson, R., Gross, M., Klemas, V., Hartman, J., 1988. Continental scale variability in vegetation reflectance and its relationship to canopy morphology. Int. J. Remote Sens. 9, 1223–1241.
Bastiaanssen, W.G., Menenti, M., Feddes, R., Holtslag, A., 1998. A remote sensing surface energy balance algorithm for land (SEBAL). 1. Formulation. *Journal of hydrology* 212, 198–212.
Bastiaanssen, W.G., Molden, D.J., Makin, I.W., 2000. Remote sensing for irrigated agriculture: examples from research and possible applications. Agric. Water Manag. 46, 137–155.
Bauriegel, E., Giebel, A., Geyer, M., Schmidt, U., Herppich, W., 2011. Early detection of Fusarium infection in wheat using hyper-spectral imaging. Comput. Electron. Agric. 75, 304–312.
Bazzi, H., Baghdadi, N., Ienco, D., El Hajj, M., Zribi, M., Belhouchette, H., Escorihuela, M.J., Demarez, V., 2019. Mapping Irrigated Areas Using Sentinel-1 Time Series in Catalonia. Spain. *Remote Sensing* 11, 1836.
Becker, F., Choudhury, B.J., 1988. Relative sensitivity of normalized difference vegetation index (NDVI) and microwave polarization difference index (MPDI) for vegetation and desertification monitoring. Remote Sens. Environ. 24, 297–311.
Benedetti, R., Rossini, P., 1993. On the use of NDVI profiles as a tool for agricultural statistics: The case study of wheat yield estimate and forecast in Emilia Romagna. Remote Sens. Environ. 45, 311–326.
Berger, K., Atzberger, C., Danner, M., D'Urso, G., Mauser, W., Vuolo, F., Hank, T., 2018. Evaluation of the PROSAIL model capabilities for future hyperspectral model environments: a review study. Remote Sensing 10, 85.
Bériaux, E., Lambot, S., Defourny, P., 2011. Estimating surface-soil moisture for retrieving maize leaf-area index from SAR data. Canadian Journal of Remote Sensing 37, 136–150.
Berry, P., Spink, J., Griffin, J., Sylvester-Bradley, R., Baker, C., Clare, R., & Scott, R. (1998). Research to understand, predict and control factors affecting lodging in wheat. Home-Grown Cereals Authority Research Project No. 169. HGCA, 131 pp.
Bhattacharya, B., Chattopadhyay, C., 2013. A multi-stage tracking for mustard rot disease combining surface meteorology and satellite remote sensing. Comput. Electron. Agric. 90, 35–44.
Biggs, T.W., Thenkabail, P.S., Gumma, M.K., Scott, C.A., Parthasaradhi, G., Turral, H., 2006. Irrigated area mapping in heterogeneous landscapes with MODIS time series, ground truth and census data, Krishna Basin, India. Int. J. Remote Sens. 27, 4245–4266.
Blaes, X., Defourny, P., 2003. Retrieving crop parameters based on tandem ERS 1/2 interferometric coherence images. Remote Sens. Environ. 88, 374–385.
Blaes, X., Defourny, P., Wegmuller, U., Della Vecchia, A., Guerriero, L., Ferrazzoli, P., 2006. C-band polarimetric indexes for maize monitoring based on a validated radiative transfer model. IEEE Trans. Geosci. Remote Sens. 44, 791–800.
Bolton, D.K., Friedl, M.A., 2013. Forecasting crop yield using remotely sensed vegetation indices and crop phenology metrics. Agric. For. Meteorol. 173, 74–84.
Bontemps, S., Defourny, P., Radoux, J., Van Bogaert, E., Lamarche, C., Achard, F., Mayaux, P., Boettcher, M., Brockmann, C., Kirches, G., 2013. Consistent global land cover maps for climate modelling communities: Current achievements of the ESA's land cover CCI. In: In, *Proceedings of the ESA Living Planet Symposium, Edimburgh*, pp. 9–13.
Boogaard, H., Van Diepen, C., Rotter, R., Cabrera, J., & Van Laar, H. (1998). WOFOST 7.1; user's guide for the WOFOST 7.1 crop growth simulation model and WOFOST Control Center 1.5. In: SC-DLO.
Bouman, B.A., van Kasteren, H.W., 1990a. Ground-based X-band (3-cm wave) radar backscattering of agricultural crops. I. Sugar beet and potato; backscattering and crop growth. Remote Sens. Environ. 34, 93–105.
Bouman, B.A., van Kasteren, H.W., 1990b. Ground-based X-band (3-cm wave) radar backscattering of agricultural crops. II. Wheat, barley, and oats; the impact of canopy structure. Remote Sens. Environ. 34, 107–119.
Bousbih, S., Zribi, M., El Hajj, M., Baghdadi, N., Lili-Chabaane, Z., Gao, Q., Fanise, P., 2018. Soil moisture and irrigation mapping in A semi-arid region, based on the synergetic use of Sentinel-1 and Sentinel-2 data. Remote Sensing 10, 1953.
Bracaglia, M., Ferrazzoli, P., Guerriero, L., 1995. A fully polarimetric multiple scattering model for crops. Remote Sens. Environ. 54, 170–179.
Brakke, T.W., Kanemasu, E.T., Steiner, J.L., Ulaby, F.T., Wilson, E., 1981. Microwave radar response to canopy moisture, leaf-area index, and dry weight of wheat, corn, and sorghum. Remote Sens. Environ. 11, 207–220.
Brisson, N., Gary, C., Justes, E., Roche, R., Mary, B., Ripoche, D., Zimmer, D., Sierra, J., Bertuzzi, P., Burger, P., 2003. An overview of the crop model STICS. Eur. J. Agron. 18, 309–332.
Brocca, L., Ciabatta, L., Massari, C., Moramarco, T., Hahn, S., Hasenauer, S., Kidd, R., Dorigo, W., Wagner, W., Levizzani, V., 2014. Soil as a natural rain gauge: Estimating global rainfall from satellite soil moisture data. J. Geophys. Res.: Atmos. 119, 5128–5141.
Brocca, L., Moramarco, T., Melone, F., Wagner, W., 2013. A new method for rainfall estimation through soil moisture observations. Geophys. Res. Lett. 40, 853–858.
Brocca, L., Pellarin, T., Crow, W.T., Ciabatta, L., Massari, C., Ryu, D., Su, C.H., Rüdiger, C., Kerr, Y., 2016. Rainfall estimation by inverting SMOS soil moisture estimates: A comparison of different methods over Australia. Journal of Geophysical Research: Atmospheres 121 12,062–012,079.
Brocca, L., Tarpanelli, A., Filippucci, P., Dorigo, W., Zaussinger, F., Gruber, A., Fernández-Prieto, D., 2018. How much water is used for irrigation? A new approach exploiting coarse resolution satellite soil moisture products. Int. J. Appl. Earth Obs. Geoinf. 73, 752–766.
Broge, N.H., Leblanc, E., 2001. Comparing prediction power and stability of broadband and hyperspectral vegetation indices for estimation of green leaf area index and canopy chlorophyll density. Remote Sens. Environ. 76, 156–172.

Brown, M., Antle, J., Backlund, P., Carr, E.R., Easterling, W., Walsh, M., Ammann, C., Attavanich, W., Barrett, C., & Bellemare, M. (2015). Climate change, global food security, and the US food system.
Cai, Y., Guan, K., Lobell, D., Potgieter, A.B., Wang, S., Peng, J., Xu, T., Asseng, S., Zhang, Y., You, L., 2019. Integrating satellite and climate data to predict wheat yield in Australia using machine learning approaches. Agric. For. Meteorol. 274, 144–159.
Calera, A., Campos, I., Osann, A., D'Urso, G., Menenti, M., 2017. Remote sensing for crop water management: from ET modelling to services for the end users. Sensors 17, 1104.
Calzadilla, A., Rehdanz, K., Betts, R., Falloon, P., Wiltshire, A., Tol, R.S., 2013. Climate change impacts on global agriculture. Clim. Change 120, 357–374.
Canisius, F., Shang, J., Liu, J., Huang, X., Ma, B., Jiao, X., Geng, X., Kovacs, J.M., Walters, D., 2018. Tracking crop phenological development using multi-temporal polarimetric Radarsat-2 data. Remote Sens. Environ. 210, 508–518.
Carruthers, I., Rosegrant, M.W., Seckler, D., 1997. Irrigation and food security in the 21st century. Irrigation and Drainage Systems 11, 83–101.
Castillejo-González, I.L., Pena-Barragán, J.M., Jurado-Expósito, M., Mesas-Carrascosa, F.J., López-Granados, F., 2014. Evaluation of pixel-and object-based approaches for mapping wild oat (Avena sterilis) weed patches in wheat fields using QuickBird imagery for site-specific management. Eur. J. Agron. 59, 57–66.
Chakrabarti, S., Bongiovanni, T., Judge, J., Zotarelli, L., Bayer, C., 2014. Assimilation of SMOS soil moisture for quantifying drought impacts on crop yield in agricultural regions. IEEE J. Sel. Top. Appl. Earth Obs. Remote Sens. 7, 3867–3879.
Chakraborty, M., Manjunath, K., Panigrahy, S., Kundu, N., Parihar, J., 2005. Rice crop parameter retrieval using multi-temporal, multi-incidence angle Radarsat SAR data. ISPRS J. Photogramm. Remote Sens. 59, 310–322.
Chakraborty, S., Newton, A.C., 2011. Climate change, plant diseases and food security: an overview. Plant. Pathol. 60, 2–14.
Chance, E., Cobourn, K., Thomas, V., 2018. Trend detection for the extent of irrigated agriculture in Idaho's Snake river plain, 1984–2016. Remote Sensing 10, 145.
Chaparro, D., Piles, M., Vall-Llossera, M., Camps, A., Konings, A.G., Entekhabi, D., 2018. L-band vegetation optical depth seasonal metrics for crop yield assessment. Remote Sens. Environ. 212, 249–259.
Chauhan, S., Darvishzadeh, R., Boschetti, M., Nelson, A., 2020. Estimation of crop angle of inclination for lodged wheat using multi-sensor SAR data. Remote Sens. Environ. 236, 111488.
Chauhan, S., Darvishzadeh, R., Boschetti, M., Pepe, M., Nelson, A., 2019a. Remote sensing-based crop lodging assessment: Current status and perspectives. ISPRS J. Photogramm. Remote Sens. 151, 124–140.
Chauhan, S., Srivastava, H.S., Patel, P., 2019b. Crop Height Estimation Using RISAT-1 Hybrid-Polarized Synthetic Aperture Radar Data. IEEE J. Sel. Top. Appl. Earth Obs. Remote Sens. 12, 2928–2933.
Chawla, I., Karthikeyan, L., Mishra, A.K., 2020. A Review of Remote Sensing Applications for Water Security: Quantity, Quality, and Extremes. J. Hydrol. 585, 124826.
Chemura, A., Mutanga, O., Dube, T., 2017. Separability of coffee leaf rust infection levels with machine learning methods at Sentinel-2 MSI spectral resolutions. Precis. Agric. 18, 859–881.
Chen, J., Lin, H., Huang, C., Fang, C., 2009. The relationship between the leaf area index (LAI) of rice and the C-band SAR vertical/horizontal (VV/HH) polarization ratio. Int. J. Remote Sens. 30, 2149–2154.
Chen, X., Dhungel, J., Bhattarai, S.P., Torabi, M., Pendergast, L., Midmore, D.J., 2011. Impact of oxygation on soil respiration, yield and water use efficiency of three crop species. J. Plant Ecol. 4 (4), 236–248.
Chen, Y., Lu, D., Luo, L., Pokhrel, Y., Deb, K., Huang, J., Ran, Y., 2018. Detecting irrigation extent, frequency, and timing in a heterogeneous arid agricultural region using MODIS time series, Landsat imagery, and ancillary data. Remote Sens. Environ. 204, 197–211.
Choudhury, B., Tucker, C., 1987. Monitoring global vegetation using Nimbus-7 37 GHz Data Some empirical relations. Int. J. Remote Sens. 8, 1085–1090.
Choudhury, B., Tucker, C., Golus, R., Newcomb, W., 1987. Monitoring vegetation using Nimbus-7 scanning multichannel microwave radiometer's data. Int. J. Remote Sens. 8, 533–538.
Chuah, H.-T., Tjuatja, S., Fung, A.K., Bredow, J.W., 1996. A phase matrix for a dense discrete random medium: Evaluation of volume scattering coefficient. IEEE Trans. Geosci. Remote Sens. 34, 1137–1143.
Ciabatta, L., Marra, A.C., Panegrossi, G., Casella, D., Sanò, P., Dietrich, S., Massari, C., Brocca, L., 2017. Daily precipitation estimation through different microwave sensors: Verification study over Italy. J. Hydrol. 545, 436–450.
Claverie, M., Matthews, J., Vermote, E., Justice, C., 2016. A 30+ year AVHRR LAI and FAPAR climate data record: Algorithm description and validation. Remote Sensing 8, 263.
Cloude, S.R., Papathanassiou, K.P., 1998. Polarimetric SAR interferometry. IEEE Trans. Geosci. Remote Sens. 36, 1551–1565.
Cloude, S.R., Chen, H., Goodenough, D.G., 2013. In: Forest height estimation and validation using Tandem-X polinsar. IEEE, pp. 1889–1892.
Collins, W., 1978. Remote sensing of crop type and maturity. Photogramm. Eng. Remote Sens. 44, 43–55.
Combal, B., Baret, F., Weiss, M., Trubuil, A., Mace, D., Pragnere, A., Myneni, R., Knyazikhin, Y., Wang, L., 2003. Retrieval of canopy biophysical variables from bi-directional reflectance: Using prior information to solve the ill-posed inverse problem. Remote Sens. Environ. 84, 1–15.
Coops, N.C., Wulder, M.A., White, J.C., 2006. Integrating remotely sensed and ancillary data sources to characterize a mountain pine beetle infestation. Remote Sens. Environ. 105, 83–97.
Crist, E.P., Cicone, R.C., 1984. A physically-based transformation of Thematic Mapper data—The TM Tasseled Cap. IEEE Trans. Geosci. Remote Sens. 256–263.
D'Odorico, P., Laio, F., Porporato, A., Ridolfi, L., Rinaldo, A., Rodriguez-Iturbe, I., 2010. Ecohydrology of terrestrial ecosystems. Bioscience 60 (11), 898–907.
da Rocha Miranda, J., de Carvalho Alves, M., Pozza, E.A., Neto, H.S., 2020. Detection of coffee berry necrosis by digital image processing of landsat 8 oli satellite imagery. Int. J. Appl. Earth Obs. Geoinf. 85, 101983.
Darvishzadeh, R., Atzberger, C., Skidmore, A., Abkar, A., 2009. Leaf Area Index derivation from hyperspectral vegetation indicesand the red edge position. Int. J. Remote Sens. 30, 6199–6218.
Das, N.N., Mohanty, B.P., 2006. Root zone soil moisture assessment using remote sensing and vadose zone modeling. Vadose Zone J. 5 (1), 296–307.
De Lannoy, G.J., Reichle, R.H., 2016. Global assimilation of multiangle and multi-polarization SMOS brightness temperature observations into the GEOS-5 catchment land surface model for soil moisture estimation. J. Hydrometeorol. 17 (2), 669–691.
De Loor, G.P., Hoogeboom, P., Attema, E.W., 1982. The dutch ROVE program. IEEE Trans. Geosci. Remote Sens. 3–11.
De Wit, A.d., & Van Diepen, C. (2007). Crop model data assimilation with the Ensemble Kalman filter for improving regional crop yield forecasts. Agricultural and forest meteorology, 146, 38-56.
Deines, J.M., Kendall, A.D., Crowley, M.A., Rapp, J., Cardille, J.A., Hyndman, D.W., 2019. Mapping three decades of annual irrigation across the US High Plains Aquifer using Landsat and Google Earth Engine. Remote Sens. Environ. 233, 111400.
Delécolle, R., Maas, S., Guérif, M., Baret, F., 1992. Remote sensing and crop production models: present trends. ISPRS J. Photogramm. Remote Sens. 47, 145–161.
Delegido, J., Verrelst, J., Meza, C., Rivera, J., Alonso, L., Moreno, J., 2013. A red-edge spectral index for remote sensing estimation of green LAI over agroecosystems. Eur. J. Agron. 46, 42–52.
Dhau, I., Dube, T., Mushore, T.D., 2019. Examining the prospects of sentinel-2 multi-spectral data in detecting and mapping maize streak virus severity in smallholder Ofcolaco farms. South Africa. *Geocarto International* 1–11.
Dheeravath, V., Thenkabail, P.S., Chandrakantha, G., Noojipady, P., Reddy, G., Biradar, C.M., Gumma, M.K., Velpuri, M., 2010. Irrigated areas of India derived using MODIS 500 m time series for the years 2001–2003. ISPRS J. Photogramm. Remote Sens. 65, 42–59.
Doell, P., Mueller Schmied, H., Schuh, C., Portmann, F.T., Eicker, A., 2014. Global-scale assessment of groundwater depletion and related groundwater abstractions: Combining hydrological modeling with information from well observations and GRACE satellites. Water Resour. Res. 50, 5698–5720.
Döll, P., Siebert, S., 2002. Global modeling of irrigation water requirements. Water Resour. Res. 38, 8-1-8-10.
Dong, T., Liu, J., Shang, J., Qian, B., Ma, B., Kovacs, J.M., Walters, D., Jiao, X., Geng, X., Shi, Y., 2019. Assessment of red-edge vegetation indices for crop leaf area index estimation. Remote Sens. Environ. 222, 133–143.
Doraiswamy, P., Hatfield, J., Jackson, T., Akhmedov, B., Prueger, J., Stern, A., 2004. Crop condition and yield simulations using Landsat and MODIS. Remote Sens. Environ. 92, 548–559.
Doraiswamy, P.C., Sinclair, T.R., Hollinger, S., Akhmedov, B., Stern, A., Prueger, J., 2005. Application of MODIS derived parameters for regional crop yield assessment. Remote Sens. Environ. 97, 192–202.
Dorigo, W.A., Zurita-Milla, R., de Wit, A.J., Brazile, J., Singh, R., Schaepman, M.E., 2007. A review on reflective remote sensing and data assimilation techniques for enhanced agroecosystem modeling. Int. J. Appl. Earth Obs. Geoinf. 9, 165–193.
Drusch, M., Moreno, J., Del Bello, U., Franco, R., Goulas, Y., Huth, A., Kraft, S., Middleton, E.M., Miglietta, F., Mohammed, G., Nedbal, L., Rascher, U., Schüttemeyer, D., Verhoef, W., 2017. The FLuorescence EXplorer mission concept - ESA's Earth Explorer 8. IEEE Trans. Geosci. Remote Sens. 55, 1273–1284.
Du, J., Kimball, J.S., Jones, L.A., 2016. Passive microwave remote sensing of soil moisture based on dynamic vegetation scattering properties for AMSR-E. IEEE Trans. Geosci. Remote Sens. 54, 597–608.
Durbha, S.S., King, R.L., Younan, N.H., 2007. Support vector machines regression for retrieval of leaf area index from multiangle imaging spectroradiometer. Remote Sens. Environ. 107, 348–361.
Easterling, W., Apps, M., 2005. Assessing the consequences of climate change for food and forest resources: a view from the IPCC. *Increasing Climate Variability and Change*. Springer, pp. 165–189.
Eckhardt, D.W., Verdin, J.P., Lyford, G.R., 1990. Automated update of an irrigated lands GIS using SPOT HRV imagery. *Photogrammetric engineering and remote sensing*. (USA).
Eklundh, L., Johansson, T., Solberg, S., 2009. Mapping insect defoliation in Scots pine with MODIS time-series data. Remote Sens. Environ. 113, 1566–1573.
Elliott, J., Deryng, D., Müller, C., Frieler, K., Konzmann, M., Gerten, D., Glotter, M., Flörke, M., Wada, Y., Best, N., 2014. Constraints and potentials of future irrigation water availability on agricultural production under climate change. Proc. Natl. Acad. Sci. 111, 3239–3244.
Engdahl, M.E., Borgeaud, M., Rast, M., 2001. The use of ERS-1/2 tandem interferometric coherence in the estimation of agricultural crop heights. IEEE Trans. Geosci. Remote Sens. 39, 1799–1806.
Erten, E., Lopez-Sanchez, J.M., Yuzugullu, O., Hajnsek, I., 2016. Retrieval of agricultural crop height from space: A comparison of SAR techniques. Remote Sens. Environ. 187, 130–144.
Escorihuela, M.J., Quintana-Seguí, P., 2016. Comparison of remote sensing and simulated soil moisture datasets in Mediterranean landscapes. Remote Sens. Environ. 180, 99–114.
Eswar, R., Sekhar, M., Bhattacharya, B., 2017. Comparison of three remote sensing based models for the estimation of latent heat flux over India. Hydrol. Sci. J. 62, 2705–2719.
Evensen, G., 2003. The ensemble Kalman filter: Theoretical formulation and practical implementation. Ocean Dyn. 53, 343–367.

Everitt, J.H., Escobar, D.E., Villarreal, R., Alaniz, M.A., Davis, M.R., 1993. Canopy light reflectance and remote sensing of shin oak (Quercus havardii) and associated vegetation. Weed Sci. 41, 291–297.
Fan, L.-Y., Gao, Y.-Z., Brück, H., Bernhofer, C., 2009. Investigating the relationship between NDVI and LAI in semi-arid grassland in Inner Mongolia using in-situ measurements. Theor. Appl. Climatol. 95, 151–156.
Fang, H., Baret, F., Plummer, S., Schaepman-Strub, G., 2019. An overview of global leaf area index (LAI): Methods, products, validation, and applications. Rev. Geophys.
Fassnacht, K.S., Gower, S.T., MacKenzie, M.D., Nordheim, E.V., Lillesand, T.M., 1997. Estimating the leaf area index of north central Wisconsin forests using the Landsat Thematic Mapper. Remote Sens. Environ. 61, 229–245.
Feret, J.-B., François, C., Asner, G.P., Gitelson, A.A., Martin, R.E., Bidel, L.P., Ustin, S.L., Le Maire, G., Jacquemoud, S., 2008. PROSPECT-4 and 5: Advances in the leaf optical properties model separating photosynthetic pigments. Remote Sens. Environ. 112, 3030–3043.
Fernandez-Moran, R., Al-Yaari, A., Mialon, A., Mahmoodi, A., Al Bitar, A., De Lannoy, G., Rodriguez-Fernandez, N., Lopez-Baeza, E., Kerr, Y., Wigneron, J.-P., 2017. SMOS-IC: An alternative SMOS soil moisture and vegetation optical depth product. Remote Sensing 9, 457.
Fieuzal, R., Duchemin, B., Jarlan, L., Zribi, M., Baup, F., Merlin, O., Hagolle, O., Garatuza-Payan, J., 2011. Combined use of optical and radar satellite data for the monitoring of irrigation and soil moisture of wheat crops. Hydrol. Earth Syst. Sci. 15, 1117–1129.
Fischer, R., 2015. Definitions and determination of crop yield, yield gaps, and of rates of change. Field Crops Research 182, 9–18.
Fitzgerald, G.J., Maas, S.J., Detar, W.R., 2004. Spider mite detection and canopy component mapping in cotton using hyperspectral imagery and spectral mixture analysis. Precis. Agric. 5, 275–289.
Fontanelli, G., Paloscia, S., Zribi, M., Chahbi, A., 2013. Sensitivity analysis of X-band SAR to wheat and barley leaf area index in the Merguellil Basin. Remote sensing letters 4, 1107–1116.
Franke, J., Menz, G., 2007. Multi-temporal wheat disease detection by multi-spectral remote sensing. Precis. Agric. 8, 161–172.
Funk, C., Budde, M.E., 2009. Phenologically-tuned MODIS NDVI-based production anomaly estimates for Zimbabwe. Remote Sens. Environ. 113, 115–125.
Gallo, K., Daughtry, C., 1987. Differences in vegetation indices for simulated Landsat-5 MSS and TM, NOAA-9 AVHRR, and SPOT-1 sensor systems. Remote Sens. Environ. 23, 439–452.
Gao, B.-C., 1996. NDWI—A normalized difference water index for remote sensing of vegetation liquid water from space. Remote Sens. Environ. 58, 257–266.
Gao, Q., Zribi, M., Escorihuela, M., Baghdadi, N., Segui, P., 2018. Irrigation mapping using Sentinel-1 time series at field scale. Remote Sensing 10, 1495.
García-Haro, F.J., Camacho, F., Martínez, B., Campos-Taberner, M., Fuster, B., Sánchez-Zapero, J., Gilabert, M.A., 2019. Climate Data Records of Vegetation Variables from Geostationary SEVIRI/MSG Data: Products. Algorithms and Applications. *Remote Sensing* 11, 2103.
Gardner, B., Blad, B., 1986. Evaluation of spectral reflectance models to estimate corn leaf area while minimizing the influence of soil background effects. Remote Sens. Environ. 20, 183–193.
Garestier, F., Dubois-Fernandez, P.C., Papathanassiou, K.P., 2007. Pine forest height inversion using single-pass X-band PolInSAR data. IEEE Trans. Geosci. Remote Sens. 46, 59–68.
Gastellu-Etchegorry, J.-P., Lauret, N., Yin, T., Landier, L., Kallel, A., Malenovský, Z., Al Bitar, A., Aval, J., Benhmida, S., Qi, J., 2017. DART: recent advances in remote sensing data modeling with atmosphere, polarization, and chlorophyll fluorescence. IEEE J. Sel. Top. Appl. Earth Obs. Remote Sens. 10, 2640–2649.
Girotto, M., Reichle, R.H., Rodell, M., Liu, Q., Mahanama, S., De Lannoy, G.J., 2019. Multi-sensor assimilation of SMOS brightness temperature and GRACE terrestrial water storage observations for soil moisture and shallow groundwater estimation. Remote Sens. Environ. 227, 12–27.
Gitelson, A.A., Gritz, Y., Merzlyak, M.N., 2003. Relationships between leaf chlorophyll content and spectral reflectance and algorithms for non-destructive chlorophyll assessment in higher plant leaves. J. Plant Physiol. 160 (3), 271–282.
Gitelson, A., Merzlyak, M.N., 1994. Spectral reflectance changes associated with autumn senescence of Aesculus hippocastanum L. and Acer platanoides L. leaves. Spectral features and relation to chlorophyll estimation. J. Plant Physiol. 143, 286–292.
Gitelson, A.A., 2004. Wide dynamic range vegetation index for remote quantification of biophysical characteristics of vegetation. J. Plant Physiol. 161, 165–173.
Gitelson, A.A., Viña, A., Ciganda, V., Rundquist, D.C., Arkebauer, T.J., 2005. Remote estimation of canopy chlorophyll content in crops. Geophys. Res. Lett. 32 (8), L08403.
Godfray, H.C.J., Beddington, J.R., Crute, I.R., Haddad, L., Lawrence, D., Muir, J.F., Pretty, J., Robinson, S., Thomas, S.M., Toulmin, C., 2010. Food security: the challenge of feeding 9 billion people. Science 327, 812–818.
Godwin, D., 1990. A user's guide to CERES Wheat V2, 10.
Gontia, N., Tiwari, K., 2008. Development of crop water stress index of wheat crop for scheduling irrigation using infrared thermometry. Agric. Water Manag. 95, 1144–1152.
Gordon, N.J., Salmond, D.J., & Smith, A.F. (1993). Novel approach to nonlinear/non-Gaussian Bayesian state estimation. In, IEE proceedings F (radar and signal processing) (pp. 107-113): IET.
Grant, J., Wigneron, J.-P., De Jeu, R., Lawrence, H., Mialon, A., Richaume, P., Al Bitar, A., Drusch, M., Van Marle, M., Kerr, Y., 2016. Comparison of SMOS and AMSR-E vegetation optical depth to four MODIS-based vegetation indices. Remote Sens. Environ. 172, 87–100.
Groten, S., 1993. NDVI—crop monitoring and early yield assessment of Burkina Faso. TitleREMOTE SENSING 14, 1495–1515.
Gu, Y., Wylie, B.K., Howard, D.M., Phuyal, K.P., Ji, L., 2013. NDVI saturation adjustment: A new approach for improving cropland performance estimates in the Greater Platte River Basin, USA. Ecol. Ind. 30, 1–6.
Guan, K., Berry, J.A., Zhang, Y., Joiner, J., Guanter, L., Badgley, G., Lobell, D.B., 2016. Improving the monitoring of crop productivity using spaceborne solar-induced fluorescence. Glob. Change Biol. 22, 716–726.
Guan, K., Wu, J., Kimball, J.S., Anderson, M.C., Frolking, S., Li, B., Hain, C.R., Lobell, D.B., 2017. The shared and unique values of optical, fluorescence, thermal and microwave satellite data for estimating large-scale crop yields. Remote Sens. Environ. 199, 333–349.
Guanter, L., Zhang, Y., Jung, M., Joiner, J., Voigt, M., Berry, J.A., Frankenberg, C., Huete, A.R., Zarco-Tejada, P., Lee, J.-E., 2014. Global and time-resolved monitoring of crop photosynthesis with chlorophyll fluorescence. Proc. Natl. Acad. Sci. 111, E1327–E1333.
Gumma, M.K., Thenkabail, P.S., Nelson, A., 2011. Mapping irrigated areas using MODIS 250 meter time-series data: A study on Krishna River Basin (India). Water 3, 113–131.
Gupta, R., Vijayan, D., Prasad, T., 2003. Comparative analysis of red-edge hyperspectral indices. Adv. Space Res. 32, 2217–2222.
Haboudane, D., Miller, J.R., Pattey, E., Zarco-Tejada, P.J., Strachan, I.B., 2004. Hyperspectral vegetation indices and novel algorithms for predicting green LAI of crop canopies: Modeling and validation in the context of precision agriculture. Remote Sens. Environ. 90, 337–352.
Hajj, M., Baghdadi, N., Belaud, G., Zribi, M., Cheviron, B., Courault, D., Hagolle, O., Charron, F., 2014. Irrigated grassland monitoring using a time series of terraSAR-X and COSMO-skyMed X-Band SAR Data. Remote Sensing 6, 10002–10032.
Han, D., Yang, H., Yang, G., & Qiu, C. (2017). Monitoring model of corn lodging based on Sentinel-1 radar image. In, 2017 SAR in Big Data Era: Models, Methods and Applications (BIGSARDATA) (pp. 1-5): IEEE.
Hanasaki, N., Inuzuka, T., Kanae, S., Oki, T., 2010. An estimation of global virtual water flow and sources of water withdrawal for major crops and livestock products using a global hydrological model. J. Hydrol. 384, 232–244.
Hanasaki, N., Kanae, S., Oki, T., 2006. A reservoir operation scheme for global river routing models. J. Hydrol. 327, 22–41.
Hansen, P., Schjoerring, J., 2003. Reflectance measurement of canopy biomass and nitrogen status in wheat crops using normalized difference vegetation indices and partial least squares regression. Remote Sens. Environ. 86, 542–553.
Harfenmeister, K., Spengler, D., Weltzien, C., 2019. Analyzing temporal and spatial characteristics of crop parameters using Sentinel-1 backscatter data. Remote Sensing 11, 1569.
Harou, J.J., Pulido-Velazquez, M., Rosenberg, D.E., Medellín-Azuara, J., Lund, J.R., Howitt, R.E., 2009. Hydro-economic models: Concepts, design, applications, and future prospects. J. Hydrol. 375, 627–643.
Hayes, M., Decker, W., 1996. Using NOAA AVHRR data to estimate maize production in the United States Corn Belt. Remote Sensing 17, 3189–3200.
Hazell, P., Wood, S., 2007. Drivers of change in global agriculture. Philosophical Transactions of the Royal Society B: Biological Sciences 363, 495–515.
He, Z., Li, S., Wang, Y., Dai, L., Lin, S., 2018. Monitoring rice phenology based on backscattering characteristics of multi-temporal RADARSAT-2 datasets. Remote Sensing 10, 340.
Heller, R.C., Johnson, K.A., 1979. Estimating irrigated land acreage from Landsat imagery [Aerial photography]. Photogramm. Eng. Remote Sens.
Herrmann, I., Pimstein, A., Karnieli, A., Cohen, Y., Alchanatis, V., Bonfil, D., 2011. LAI assessment of wheat and potato crops by VENμS and Sentinel-2 bands. Remote Sens. Environ. 115, 2141–2151.
Hofius, D., Börnke, F.A., 2007. Photosynthesis, carbohydrate metabolism and source–sink relations. *Potato Biology and Biotechnology*. Elsevier, pp. 257–285.
Holzapfel, C., Lafond, G., Brandt, S., Bullock, P., Irvine, R., Morrison, M., May, W., James, D., 2009. Estimating canola (Brassica napus L.) yield potential using an active optical sensor. Can. J. Plant Sci. 89, 1149–1160.
Holzworth, D.P., Huth, N.I., deVoil, P.G., Zurcher, E.J., Herrmann, N.I., McLean, G., Chenu, K., van Oosterom, E.J., Snow, V., Murphy, C., 2014. APSIM–evolution towards a new generation of agricultural systems simulation. Environ. Modell. Software 62, 327–350.
Hoogenboom, G., Porter, C.H., Shelia, V., Boote, K.J., Singh, U., White, J.W., Hunt, L.A., Ogoshi, R., Lizaso, J.I., Koo, J., Asseng, S., Singles, A., Moreno, L.P., & Jones, J.W. (2019). Decision Support System for Agrotechnology Transfer (DSSAT) Version 4.7.5 (https://DSSAT.net). In. DSSAT Foundation, Gainesville, Florida, USA.
Hornbuckle, B.K., Patton, J.C., VanLoocke, A., Suyker, A.E., Roby, M.C., Walker, V.A., Iyer, E.R., Herzmann, D.E., Endacott, E.A., 2016. SMOS optical thickness changes in response to the growth and development of crops, crop management, and weather. Remote Sens. Environ. 180, 320–333.
Hosseini, M., McNairn, H., Merzouki, A., Pacheco, A., 2015. Estimation of Leaf Area Index (LAI) in corn and soybeans using multi-polarization C-and L-band radar data. Remote Sens. Environ. 170, 77–89.
Houborg, R., Soegaard, H., Boegh, E., 2007. Combining vegetation index and model inversion methods for the extraction of key vegetation biophysical parameters using Terra and Aqua MODIS reflectance data. Remote Sens. Environ. 106, 39–58.
Hsiao, T.C., 1973. Plant responses to water stress. Annu. Rev. Plant Physiol. 24 (1), 519–570.
Hu, J., Liu, L., Guo, J., Du, S., Liu, X., 2018. Upscaling Solar-Induced Chlorophyll Fluorescence from an Instantaneous to Daily Scale Gives an Improved Estimation of the Gross Primary Productivity. Remote Sensing 10, 1663.
Huang, J., Gómez-Dans, J.L., Huang, H., Ma, H., Wu, Q., Lewis, P.E., Liang, S., Chen, Z., Xue, J.-H., Wu, Y., 2019. Assimilation of remote sensing into crop growth models: Current status and perspectives. Agric. For. Meteorol. 276, 107609.

Huang, W., Guan, Q., Luo, J., Zhang, J., Zhao, J., Liang, D., Huang, L., Zhang, D., 2014. New optimized spectral indices for identifying and monitoring winter wheat diseases. IEEE J. Sel. Top. Appl. Earth Obs. Remote Sens. 7, 2516–2524.

Iio, A., Hikosaka, K., Anten, N.P., Nakagawa, Y., Ito, A., 2014. Global dependence of field-observed leaf area index in woody species on climate: a systematic review. Glob. Ecol. Biogeogr. 23, 274–285.

Ines, A.V., Das, N.N., Hansen, J.W., Njoku, E.G., 2013. Assimilation of remotely sensed soil moisture and vegetation with a crop simulation model for maize yield prediction. Remote Sens. Environ. 138, 149–164.

Inoue, Y., Kurosu, T., Maeno, H., Uratsuka, S., Kozu, T., Dabrowska-Zielinska, K., Qi, J., 2002. Season-long daily measurements of multifrequency (Ka, Ku, X, C, and L) and full-polarization backscatter signatures over paddy rice field and their relationship with biological variables. Remote Sens. Environ. 81, 194–204.

Inoue, Y., Sakaiya, E., Wang, C., 2014. Capability of C-band backscattering coefficients from high-resolution satellite SAR sensors to assess biophysical variables in paddy rice. Remote Sens. Environ. 140, 257–266.

Jackson, R.D., Idso, S., Reginato, R., Pinter Jr, P., 1981. Canopy temperature as a crop water stress indicator. Water Resour. Res. 17, 1133–1138.

Jacquemoud, S., Baret, F., 1990. PROSPECT: A model of leaf optical properties spectra. Remote Sens. Environ. 34, 75–91.

Jacquemoud, S., Verhoef, W., Baret, F., Bacour, C., Zarco-Tejada, P.J., Asner, G.P., François, C., Ustin, S.L., 2009. PROSPECT+ SAIL models: A review of use for vegetation characterization. Remote Sens. Environ. 113, S56–S66.

Jalilvand, E., Tajrishy, M., Hashemi, S.A.G.Z., Brocca, L., 2019. Quantification of irrigation water using remote sensing of soil moisture in a semi-arid region. Remote Sens. Environ. 231, 111226.

Jeong, S., Kang, S., Jang, K., Lee, H., Hong, S., Ko, D., 2012. Development of Variable Threshold Models for detection of irrigated paddy rice fields and irrigation timing in heterogeneous land cover. Agric. Water Manag. 115, 83–91.

Ji, R., Xie, B.-Y., Li, D.-M., Li, Z., Zhang, X., 2004. Use of MODIS data to monitor the oriental migratory locust plague. Agric. Ecosyst. Environ. 104, 615–620.

Jiang, Z., Huete, A.R., Didan, K., Miura, T., 2008. Development of a two-band enhanced vegetation index without a blue band. Remote Sens. Environ. 112, 3833–3845.

Jiao, X., McNairn, H., Shang, J., Pattey, E., Liu, J., Champagne, C., 2011. The sensitivity of RADARSAT-2 polarimetric SAR data to corn and soybean leaf area index. Canadian Journal of Remote Sensing 37, 69–81.

Jin, N., Tao, B., Ren, W., Feng, M., Sun, R., He, L., Zhuang, W., Yu, Q., 2016. Mapping irrigated and rainfed wheat areas using multi-temporal satellite data. Remote Sensing 8, 207.

Jin, X., Kumar, L., Li, Z., Feng, H., Xu, X., Yang, G., Wang, J., 2018. A review of data assimilation of remote sensing and crop models. Eur. J. Agron. 92, 141–152.

Johnson, D.M., 2014. An assessment of pre-and within-season remotely sensed variables for forecasting corn and soybean yields in the United States. Remote Sens. Environ. 141, 116–128.

Johnson, L.F., 2003. Temporal stability of an NDVI-LAI relationship in a Napa Valley vineyard. Aust. J. Grape Wine Res. 9, 96–101.

Johnson, M.D., Hsieh, W.W., Cannon, A.J., Davidson, A., Bédard, F., 2016. Crop yield forecasting on the Canadian Prairies by remotely sensed vegetation indices and machine learning methods. Agric. For. Meteorol. 218, 74–84.

Jones, J.W., Hoogenboom, G., Porter, C.H., Boote, K.J., Batchelor, W.D., Hunt, L., Wilkens, P.W., Singh, U., Gijsman, A.J., Ritchie, J.T., 2003. The DSSAT cropping system model. Eur. J. Agron. 18, 235–265.

Jones, M.O., Jones, L.A., Kimball, J.S., McDonald, K.C., 2011. Satellite passive microwave remote sensing for monitoring global land surface phenology. Remote Sens. Environ. 115, 1102–1114.

Kalman, R.E., 1960. A new approach to linear filtering and prediction problems. J. Basic Eng. 82, 35–45.

Kamthonkiat, D., Honda, K., Turral, H., Tripathi, N., Wuwongse, V., 2005. Discrimination of irrigated and rainfed rice in a tropical agricultural system using SPOT VEGETATION NDVI and rainfall data. Int. J. Remote Sens. 26, 2527–2547.

Karam, M.A., Amar, F., Fung, A.K., Mougin, E., Lopes, A., Le Vine, D.M., Beaudoin, A., 1995. A microwave polarimetric scattering model for forest canopies based on vector radiative transfer theory. Remote Sens. Environ. 53, 16–30.

Karam, M.A., Fung, A.K., Lang, R.H., Chauhan, N.S., 1992. A microwave scattering model for layered vegetation. IEEE Trans. Geosci. Remote Sens. 30, 767–784.

Karthikeyan, L., Pan, M., Konings, A.G., Piles, M., Fernandez-Moran, R., Kumar, D.N., Wood, E.F., 2019. Simultaneous retrieval of global scale Vegetation Optical Depth, surface roughness, and soil moisture using X-band AMSR-E observations. Remote Sens. Environ. 234, 111473.

Karthikeyan, L., Pan, M., Wanders, N., Kumar, D.N., Wood, E.F., 2017. Four decades of microwave satellite soil moisture observations: Part 1. A review of retrieval algorithms. Adv. Water Resour. 109, 106–120.

Kendall, S., Holmes, H., White, C., Clarke, S., Berry, P., 2017. Quantifying lodging-induced yield losses in oilseed rape. Field Crops Research 211, 106–113.

Khati, U., Singh, G., Ferro-Famil, L., 2017. Analysis of seasonal effects on forest parameter estimation of Indian deciduous forest using TerraSAR-X PolInSAR acquisitions. Remote Sens. Environ. 199, 265–276.

Khati, U., Singh, G., Kumar, S., 2018. Potential of Space-Borne PolInSAR for Forest Canopy Height Estimation Over India—A Case Study Using Fully PolarimetricL-, C-, andX-Band SAR Data. IEEE J. Sel. Top. Appl. Earth Obs. Remote Sens. 11, 2406–2416.

Kim, Y., van Zyl, J.J., 2009. A time-series approach to estimate soil moisture using polarimetric radar data. IEEE Trans. Geosci. Remote Sens. 47, 2519–2527.

Kilic, L., Prigent, C., Aires, F., Boutin, J., Heygster, G., Tonboe, R.T., Roquet, H., Jimenez, C., Donlon, C., 2018. Expected Performances of the Copernicus Imaging Microwave Radiometer (CIMR) for an All-Weather and High Spatial Resolution Estimation of Ocean and Sea Ice Parameters. J. Geophys. Res.: Oceans 123, 7564–7580.

Kim, Y., Jackson, T., Bindlish, R., Lee, H., Hong, S., 2011. Radar vegetation index for estimating the vegetation water content of rice and soybean. IEEE Geosci. Remote Sens. Lett. 9, 564–568.

Kira, O., Nguy-Robertson, A.L., Arkebauer, T.J., Linker, R., Gitelson, A.A., 2016. Informative spectral bands for remote green LAI estimation in C3 and C4 crops. Agric. For. Meteorol. 218, 243–249.

Klein Goldewijk, K., Beusen, A., Janssen, P., 2010. Long-term dynamic modeling of global population and built-up area in a spatially explicit way: HYDE 3.1. The Holocene 20, 565–573.

Kogan, F.N., 1995. Application of vegetation index and brightness temperature for drought detection. Adv. Space Res. 15 (11), 91–100.

Konings, A.G., Piles, M., Das, N., Entekhabi, D., 2017. L-band vegetation optical depth and effective scattering albedo estimation from SMAP. Remote Sens. Environ. 198, 460–470.

Konings, A.G., Piles, M., Rötzer, K., McColl, K.A., Chan, S.K., Entekhabi, D., 2016. Vegetation optical depth and scattering albedo retrieval using time series of dual-polarized L-band radiometer observations. Remote Sens. Environ. 172, 178–189.

Krieger, G., Moreira, A., Fiedler, H., Hajnsek, I., Werner, M., Younis, M., Zink, M., 2007. TanDEM-X: A satellite formation for high-resolution SAR interferometry. IEEE Trans. Geosci. Remote Sens. 45, 3317–3341.

Kroes, J., Van Dam, J., Groenendijk, P., Hendriks, R., & Jacobs, C. (2009). SWAP version 3.2. Theory description and user manual. In: Alterra.

Kumar, S., Peters-Lidard, C., Santanello, J., Reichle, R., Draper, C., Koster, R., Nearing, G., & Jasinski, M. (2015). Evaluating the utility of satellite soil moisture retrievals over irrigated areas and the ability of land data assimilation methods to correct for unmodeled processes.

Labus, M., Nielsen, G., Lawrence, R., Engel, R., Long, D., 2002. Wheat yield estimates using multi-temporal NDVI satellite imagery. Int. J. Remote Sens. 23, 4169–4180.

Lai, Y., Pringle, M., Kopittke, P.M., Menzies, N.W., Orton, T.G., Dang, Y.P., 2018. An empirical model for prediction of wheat yield, using time-integrated Landsat NDVI. Int. J. Appl. Earth Obs. Geoinf. 72, 99–108.

Lawrence, H., Wigneron, J.-P., Richaume, P., Novello, N., Grant, J., Mialon, A., Al Bitar, A., Merlin, O., Guyon, D., Leroux, D., 2014. Comparison between SMOS Vegetation Optical Depth products and MODIS vegetation indices over crop zones of the USA. Remote Sens. Environ. 140, 396–406.

Lawston, P.M., Santanello Jr, J.A., Kumar, S.V., 2017. Irrigation signals detected from SMAP soil moisture retrievals. Geophys. Res. Lett. 44 11,860–811,867.

Le Toan, T., Ribbes, F., Wang, L.-F., Floury, N., Ding, K.-H., Kong, J.A., Fujita, M., Kurosu, T., 1997. Rice crop mapping and monitoring using ERS-1 data based on experiment and modeling results. IEEE Trans. Geosci. Remote Sens. 35, 41–56.

Le Vine, D., Schneider, A., Lang, R., Carter, H., 1985. Scattering from thin dielectric disks. IEEE Trans. Antennas Propag. 33, 1410–1413.

Lee, K.-S., Cohen, W.B., Kennedy, R.E., Maiersperger, T.K., Gower, S.T., 2004. Hyperspectral versus multispectral data for estimating leaf area index in four different biomes. Remote Sens. Environ. 91, 508–520.

Lee, S.-K., Yoon, S., Won, J.-S., 2018. Vegetation Height Estimate in Rice Fields Using Single Polarization TanDEM-X Science Phase Data. Remote Sensing 10, 1702.

Lettenmaier, D.P., Alsdorf, D., Dozier, J., Huffman, G.J., Pan, M., Wood, E.F., 2015. Inroads of remote sensing into hydrologic science during the WRR era. Water Resour. Res. 51 (9), 7309–7342.

Li, F., Crow, W.T., Kustas, W.P., 2010. Towards the estimation root-zone soil moisture via the simultaneous assimilation of thermal and microwave soil moisture retrievals. Adv. Water Resour. 33 (2), 201–214.

Li, H., Han, Y., Chen, J., 2019. Capability of multidate RADARSAT-2 data to identify sugarcane lodging. J. Appl. Remote Sens. 13, 044514.

Li, H., Liu, G., Liu, Q., Chen, Z., Huang, C., 2018. Retrieval of winter wheat leaf area index from Chinese GF-1 satellite data using the PROSAIL model. Sensors 18, 1120.

Li, X., Zhang, Y., Bao, Y., Luo, J., Jin, X., Xu, X., Song, X., Yang, G., 2014. Exploring the best hyperspectral features for LAI estimation using partial least squares regression. Remote Sensing 6, 6221–6241.

Li, Z., Jin, X., Wang, J., Yang, G., Nie, C., Xu, X., Feng, H., 2015. Estimating winter wheat (Triticum aestivum) LAI and leaf chlorophyll content from canopy reflectance data by integrating agronomic prior knowledge with the PROSAIL model. Int. J. Remote Sens. 36, 2634–2653.

Liang, L., Di, L., Zhang, L., Deng, M., Qin, Z., Zhao, S., Lin, H., 2015. Estimation of crop LAI using hyperspectral vegetation indices and a hybrid inversion method. Remote Sens. Environ. 165, 123–134.

Liu, D., Mishra, A.K., 2017. Performance of AMSR_E soil moisture data assimilation in CLM4. 5 model for monitoring hydrologic fluxes at global scale. J. Hydrol. 547, 67–79.

Liu, D., Mishra, A.K., Yu, Z., 2019a. Evaluation of hydroclimatic variables for maize yield estimation using crop model and remotely sensed data assimilation. Stoch. Env. Res. Risk Assess. 33, 1283–1295.

Liu, H.Q., Huete, A., 1995. A feedback based modification of the NDVI to minimize canopy background and atmospheric noise. IEEE Trans. Geosci. Remote Sens. 33, 457–465.

Liu, J., Miller, J.R., Haboudane, D., & Pattey, E. (2004). Exploring the relationship between red edge parameters and crop variables for precision agriculture. In, IGARSS 2004. 2004 IEEE International Geoscience and Remote Sensing Symposium (pp. 1276-1279): IEEE.

Liu, L., Dong, Y., Huang, W., Du, X., Luo, J., Shi, Y., Ma, H., 2019b. Enhanced Regional Monitoring of Wheat Powdery Mildew Based on an Instance-Based Transfer Learning Method. Remote sensing 11, 298.

Liu, L., Guan, L., Liu, X., 2017. Directly estimating diurnal changes in GPP for C3 and C4 crops using far-red sun-induced chlorophyll fluorescence. Agric. For. Meteorol. 232, 1–9.

Liu, W., Kogan, F., 2002. Monitoring Brazilian soybean production using NOAA/AVHRR based vegetation condition indices. Int. J. Remote Sens. 23, 1161–1179.
Liu, Y.Y., de Jeu, R.A., McCabe, M.F., Evans, J.P., & van Dijk, A.I. (2011). Global long--term passive microwave satellite-based retrievals of vegetation optical depth. Geophysical Research Letters, 38.
Lopez-Sanchez, J.M., Ballester-Berman, J.D., Hajnsek, I., 2010. First results of rice monitoring practices in Spain by means of time series of TerraSAR-X dual-pol images. IEEE J. Sel. Top. Appl. Earth Obs. Remote Sens. 4, 412–422.
Lopez-Sanchez, J.M., Ballester-Berman, J.D., Marquez-Moreno, Y., 2007. Model limitations and parameter-estimation methods for agricultural applications of polarimetric SAR interferometry. IEEE Trans. Geosci. Remote Sens. 45, 3481–3493.
Lopez-Sanchez, J.M., Hajnsek, I., Ballester-Berman, J.D., 2011. First demonstration of agriculture height retrieval with PolInSAR airborne data. IEEE Geosci. Remote Sens. Lett. 9, 242–246.
Lopez-Sanchez, J.M., Vicente-Guijalba, F., Erten, E., Campos-Taberner, M., Garcia-Haro, F.J., 2017. Retrieval of vegetation height in rice fields using polarimetric SAR interferometry with TanDEM-X data. Remote Sens. Environ. 192, 30–44.
Lunetta, R.S., Shao, Y., Ediriwickrema, J., Lyon, J.G., 2010. Monitoring agricultural cropping patterns across the Laurentian Great Lakes Basin using MODIS-NDVI data. Int. J. Appl. Earth Obs. Geoinf. 12, 81–88.
Luo, J., Huang, W., Zhao, J., Zhang, J., Zhao, C., Ma, R., 2013. Detecting aphid density of winter wheat leaf using hyperspectral measurements. IEEE J. Sel. Top. Appl. Earth Obs. Remote Sens. 6, 690–698.
Ma, B., Dwyer, L.M., Costa, C., Cober, E.R., Morrison, M.J., 2001. Early prediction of soybean yield from canopy reflectance measurements. Agron. J. 93, 1227–1234.
Macelloni, G., Paloscia, S., Pampaloni, P., Marliani, F., Gai, M., 2001. The relationship between the backscattering coefficient and the biomass of narrow and broad leaf crops. IEEE Trans. Geosci. Remote Sens. 39, 873–884.
Major, D., Smith, A., Hill, M., Willms, W., Brisco, B., & Brown, R. (1994). Radar backscatter and visible infrared reflectance from short-grass prairie.
Malbeteau, Y., Merlin, O., Balsamo, G., Er-Raki, S., Khabba, S., Walker, J., Jarlan, L., 2018. Toward a surface soil moisture product at high spatiotemporal resolution: temporally interpolated, spatially disaggregated SMOS data. J. Hydrometeorol. 19, 183–200.
Manavalan, P., Kesavasamy, K., Adiga, S., 1995. Irrigated crops monitoring through seasons using digital change detection analysis of IRS-LISS 2 data. Int. J. Remote Sens. 16, 633–640.
Mandal, D., Hosseini, M., McNairn, H., Kumar, V., Bhattacharya, A., Rao, Y., Mitchell, S., Robertson, L.D., Davidson, A., Dabrowska-Zielinska, K., 2019a. An investigation of inversion methodologies to retrieve the leaf area index of corn from C-band SAR data. Int. J. Appl. Earth Obs. Geoinf. 82, 101893.
Mandal, D., Kumar, V., McNairn, H., Bhattacharya, A., Rao, Y., 2019b. Joint estimation of Plant Area Index (PAI) and wet biomass in wheat and soybean from C-band polarimetric SAR data. Int. J. Appl. Earth Obs. Geoinf. 79, 24–34.
Mariotto, I., Thenkabail, P.S., Huete, A., Slonecker, E.T., Platonov, A., 2013. Hyperspectral versus multispectral crop-productivity modeling and type discrimination for the HyspIRI mission. Remote Sens. Environ. 139, 291–305.
Martens, B., Gonzalez Miralles, D., Lievens, H., Van Der Schalie, R., De Jeu, R.A., Fernández-Prieto, D., Verhoest, N., 2017. GLEAM v3: Satellite-based land evaporation and root-zone soil moisture. Geosci. Model Dev. 10 (5), 1903–1925.
Mateo-Sanchis, A., Piles, M., Muñoz-Marí, J., Adsuara, J.E., Pérez-Suay, A., Camps-Valls, G., 2019. Synergistic integration of optical and microwave satellite data for crop yield estimation. Remote Sens. Environ. 234, 111460.
Matongera, T.N., Mutanga, O., Dube, T., Sibanda, M., 2017. Detection and mapping the spatial distribution of bracken fern weeds using the Landsat 8 OLI new generation sensor. Int. J. Appl. Earth Obs. Geoinf. 57, 93–103.
Meier, J., Zabel, F., Mauser, W., 2018. A global approach to estimate irrigated areas–a comparison between different data and statistics. Hydrol. Earth Syst. Sci. 22, 1119–1133.
Meroni, M., Rossini, M., Guanter, L., Alonso, L., Rascher, U., Colombo, R., Moreno, J., 2009. Remote sensing of solar-induced chlorophyll fluorescence: Review of methods and applications. Remote Sens. Environ. 113, 2037–2051.
Migdall, S., Bach, H., Bobert, J., Wehrhan, M., Mauser, W., 2009. Inversion of a canopy reflectance model using hyperspectral imagery for monitoring wheat growth and estimating yield. Precis. Agric. 10, 508.
Miller, J.R., Berger, M., Alonso, L., Cerovic, Z., Goulas, Y., Jacquemoud, S., Louis, J., Mohammed, G., Moya, I., & Pedros, R. (2003). Progress on the development of an integrated canopy fluorescence model. In, IGARSS 2003. 2003 IEEE International Geoscience and Remote Sensing Symposium. Proceedings (IEEE Cat. No. 03CH37477) (pp. 601-603): IEEE.
Mirasi, A., Mahmoudi, A., Navid, H., Valizadeh Kamran, K., Asoodar, M.A., 2019. Evaluation of sum-NDVI values to estimate wheat grain yields using multi-temporal Landsat OLI data. Geocarto International, pp. 1–16.
Mkhabela, M., Bullock, P., Raj, S., Wang, S., Yang, Y., 2011. Crop yield forecasting on the Canadian Prairies using MODIS NDVI data. Agric. For. Meteorol. 151, 385–393.
Mladenova, I.E., Bolten, J.D., Crow, W.T., Anderson, M.C., Hain, C.R., Johnson, D.M., Mueller, R., 2017. Intercomparison of soil moisture, evaporative stress, and vegetation indices for estimating corn and soybean yields over the US. IEEE J. Sel. Top. Appl. Earth Obs. Remote Sens. 10, 1328–1343.
Moesinger, L., Dorigo, W., de Jeu, R., van der Schalie, R., Scanlon, T., Teubner, I., Forkel, M., 2019. The Global Long-term Microwave Vegetation Optical Depth Climate Archive VODCA. Sci. Data Discuss, Earth Syst in review.
Mohammed, G.H., Colombo, R., Middleton, E.M., Rascher, U., van der Tol, C., Nedbal, L., Goulas, Y., Pérez-Priego, O., Damm, A., Meroni, M., 2019. Remote sensing of solar-induced chlorophyll fluorescence (SIF) in vegetation: 50 years of progress. Remote Sens. Environ. 231, 111177.
Monteith, J.L., 1977. Climate and the efficiency of crop production in Britain. *Philosophical Transactions of the Royal Society of London*. B, Biological Sciences 281, 277–294.
Motohka, T., Nasahara, K.N., Oguma, H., Tsuchida, S., 2010. Applicability of green-red vegetation index for remote sensing of vegetation phenology. Remote Sensing 2, 2369–2387.
Mulla, D.J., 2013. Twenty five years of remote sensing in precision agriculture: Key advances and remaining knowledge gaps. Biosyst. Eng. 114, 358–371.
Müllerová, J., Brůna, J., Bartaloš, T., Dvořák, P., Vítková, M., Pyšek, P., 2017. Timing is important: unmanned aircraft vs. satellite imagery in plant invasion monitoring. *Frontiers in plant science* 8, 887.
Myneni, R., & Knyazikhin, Y. (2018). VIIRS/NPP Leaf Area Index/FPAR 8-Day L4 Global 500m SIN Grid V001. In N.E.L.P. DAAC (Ed.).
Myneni, R., Knyazikhin, Y., Park, T., 2015. MCD15A3H MODIS/Terra + Aqua Leaf Area Index/FPAR 4-day L4 Global 500 m SIN Grid V006. Land Processes DAAC.
Myneni, R.B., Hoffman, S., Knyazikhin, Y., Privette, J., Glassy, J., Tian, Y., Wang, Y., Song, X., Zhang, Y., Smith, G., 2002. Global products of vegetation leaf area and fraction absorbed PAR from year one of MODIS data. Remote Sens. Environ. 83, 214–231.
Nair, A.S., Indu, J., 2019. Improvement of land surface model simulations over India via data assimilation of satellite-based soil moisture products. J. Hydrol. 573, 406–421.
Nendel, C., Berg, M., Kersebaum, K.C., Mirschel, W., Specka, X., Wegehenkel, M., Wenkel, K., Wieland, R., 2011. The MONICA model: Testing predictability for crop growth, soil moisture and nitrogen dynamics. Ecol. Model. 222, 1614–1625.
Nguyen, H.T., Lee, B.-W., 2006. Assessment of rice leaf growth and nitrogen status by hyperspectral canopy reflectance and partial least square regression. Eur. J. Agron. 24, 349–356.
Nhamo, L., Ebrahim, G.Y., Mabhaudhi, T., Mpandeli, S., Magombeyi, M., Chitakira, M., Magidi, J., Sibanda, M., 2019. An assessment of groundwater use in irrigated agriculture using multi-spectral remote sensing. Physics and Chemistry of the Earth, Parts A/B/C, pp. 102810.
Nilsen, E.T., Orcutt, D.M., 1996. Physiology of plants under stress. Wiley, Abiotic factors.
Norman, J.M., Kustas, W.P., Humes, K.S., 1995. Source approach for estimating soil and vegetation energy fluxes in observations of directional radiometric surface temperature. Agric. For. Meteorol. 77, 263–293.
Norton, A.J., Rayner, P.J., Koffi, E.N., Scholze, M., 2018. Assimilating solar-induced chlorophyll fluorescence into the terrestrial biosphere model BETHY-SCOPE v1. 0: model description and information content. Geosci. Model Dev. 11, 1517–1536.
O'Neill, P., Chan, S., Njoku, E., Jackson, T., & Bindlish, R. (2018). Algorithm Theoretical Basis Document Level 2 & 3 Soil Moisture (Passive) Data Products; Revision D. Jet Propulsion Lab., California Inst. Technol.: Pasadena, CA, USA.
Odindi, J.O., Adam, E.E., Ngubane, Z., Mutanga, O., Slotow, R., 2014. Comparison between WorldView-2 and SPOT-5 images in mapping the bracken fern using the random forest algorithm. J. Appl. Remote Sens. 8, 083527.
Oerke, E.-C., 2006. Crop losses to pests. The Journal of Agricultural Science 144, 31–43.
Oki, T., Kanae, S., 2006. Global hydrological cycles and world water resources. Science 313, 1068–1072.
O'Shaughnessy, S.A., Evett, S.R., Colaizzi, P.D., Howell, T.A., 2012. A crop water stress index and time threshold for automatic irrigation scheduling of grain sorghum. Agric. Water Manag. 107, 122–132.
Otter-Nacke, S., Ritchie, J., Godwin, D., & Singh, U. (1991). A Users Guide to CERES Barley v. 2.10. International Fertilizer Development Center, Muscle Shoals, AL.
Ottosen, T.-B., Lommen, S.T., Skjøth, C.A., 2019. Remote sensing of cropping practice in Northern Italy using time-series from Sentinel-2. Comput. Electron. Agric. 157, 232–238.
Oumar, Z., Mutanga, O., 2013. Using WorldView-2 bands and indices to predict bronze bug (Thaumastocoris peregrinus) damage in plantation forests. Int. J. Remote Sens. 34, 2236–2249.
Owe, M., de Jeu, R., Walker, J., 2001. A methodology for surface soil moisture and vegetation optical depth retrieval using the microwave polarization difference index. IEEE Trans. Geosci. Remote Sens. 39, 1643–1654.
Ozdogan, M. (2011). Exploring the potential contribution of irrigation to global agricultural primary productivity. Global biogeochemical cycles, 25.
Ozdogan, M., Gutman, G., 2008. A new methodology to map irrigated areas using multi-temporal MODIS and ancillary data: An application example in the continental US. Remote Sens. Environ. 112, 3520–3537.
Ozdogan, M., Woodcock, C.E., Salvucci, G.D., Demir, H., 2006. Changes in summer irrigated crop area and water use in Southeastern Turkey from 1993 to 2002: Implications for current and future water resources. Water Resour. Manage. 20, 467–488.
Ozdogan, M., Yang, Y., Allez, G., Cervantes, C., 2010. Remote sensing of irrigated agriculture: Opportunities and challenges. Remote Sensing 2, 2274–2304.
Pacheco-Labrador, J., Perez-Priego, O., El-Madany, T.S., Julitta, T., Rossini, M., Guan, J., Moreno, G., Carvalhais, N., Martín, M.P., Gonzalez-Cascon, R., 2019. Multiple-constraint inversion of SCOPE. Evaluating the potential of GPP and SIF for the retrieval of plant functional traits. Remote Sens. Environ. 234, 111362.
Paloscia, S., 1998. An empirical approach to estimating leaf area index from multi-frequency SAR data. Int. J. Remote Sens. 19, 359–364.
Paloscia, S., Pampaloni, P., 1992. Microwave vegetation indexes for detecting biomass and water conditions of agricultural crops. Remote Sens. Environ. 40, 15–26.
Panda, S.S., Ames, D.P., Panigrahi, S., 2010. Application of vegetation indices for agricultural crop yield prediction using neural network techniques. Remote Sensing 2, 673–696.
Papathanassiou, K.P., Cloude, S.R., 2001. Single-baseline polarimetric SAR interferometry. IEEE Trans. Geosci. Remote Sens. 39, 2352–2363.
Patton, J., Hornbuckle, B., 2012. Initial validation of SMOS vegetation optical thickness in

Iowa. IEEE Geosci. Remote Sens. Lett. 10, 647–651.
Paul-Limoges, E., Damm, A., Hueni, A., Liebisch, F., Eugster, W., Schaepman, M.E., Buchmann, N., 2018. Effect of environmental conditions on sun-induced fluorescence in a mixed forest and a cropland. Remote Sens. Environ. 219, 310–323.
Pearson, R.L., Miller, L.D., 1972. Remote mapping of standing crop biomass for estimation of the productivity of the shortgrass prairie. In, *Remote sensing of environment* VIII, (p. 1355).
Peña-Arancibia, J.L., McVicar, T.R., Paydar, Z., Li, L., Guerschman, J.P., Donohue, R.J., Dutta, D., Podger, G.M., van Dijk, A.I., Chiew, F.H., 2014. Dynamic identification of summer cropping irrigated areas in a large basin experiencing extreme climatic variability. Remote Sens. Environ. 154, 139–152.
Pengra, B.W., Johnston, C.A., Loveland, T.R., 2007. Mapping an invasive plant, Phragmites australis, in coastal wetlands using the EO-1 Hyperion hyperspectral sensor. Remote Sens. Environ. 108, 74–81.
Pervez, M.S., Budde, M., Rowland, J., 2014. Mapping irrigated areas in Afghanistan over the past decade using MODIS NDVI. Remote Sens. Environ. 149, 155–165.
Peters, A.J., Reed, B.C., Eve, M.D., McDaniel, K.C., 1992. Remote sensing of broom snakeweed (Gutierrezia sarothrae) with NOAA-10 spectral image processing. Weed Technol. 6, 1015–1020.
Pichierri, M., Hajnsek, I., 2017. Comparing performances of crop height inversion schemes from multifrequency pol-InSAR data. IEEE J. Sel. Top. Appl. Earth Obs. Remote Sens. 10, 1727–1741.
Piles, M., Camps-Valls, G., Chaparro, D., Entekhabi, D., Konings, A.G., & Jagdhuber, T. (2017). Remote sensing of vegetation dynamics in agro-ecosystems using SMAP vegetation optical depth and optical vegetation indices. In, 2017 IEEE International Geoscience and Remote Sensing Symposium (IGARSS) (pp. 4346-4349): IEEE.
Pinthus, M.J., 1974. Lodging in wheat, barley, and oats: the phenomenon, its causes, and preventive measures. *Advances in agronomy*. Elsevier, pp. 209–263.
Pokhrel, Y., Hanasaki, N., Koirala, S., Cho, J., Yeh, P.J.-F., Kim, H., Kanae, S., Oki, T., 2012. Incorporating anthropogenic water regulation modules into a land surface model. J. Hydrometeorol. 13, 255–269.
Portmann, F.T., Siebert, S., & Döll, P. (2010). MIRCA2000—Global monthly irrigated and rainfed crop areas around the year 2000: A new high-resolution data set for agricultural and hydrological modeling. Global biogeochemical cycles, 24.
Prabhakar, M., Prasad, Y., Thirupathi, M., Sreedevi, G., Dharajothi, B., Venkateswarlu, B., 2011. Use of ground based hyperspectral remote sensing for detection of stress in cotton caused by leafhopper (Hemiptera: Cicadellidae). Comput. Electron. Agric. 79, 189–198.
Prasad, A.K., Chai, L., Singh, R.P., Kafatos, M., 2006. Crop yield estimation model for Iowa using remote sensing and surface parameters. Int. J. Appl. Earth Obs. Geoinf. 8, 26–33.
Prince, S., 1991. A model of regional primary production for use with coarse resolution satellite data. Int. J. Remote Sens. 12, 1313–1330.
Qiu, J., Gao, Q., Wang, S., Su, Z., 2016. Comparison of temporal trends from multiple soil moisture data sets and precipitation: The implication of irrigation on regional soil moisture trend. Int. J. Appl. Earth Obs. Geoinf. 48, 17–27.
Quarmby, N., Milnes, M., Hindle, T., Silleos, N., 1993. The use of multi-temporal NDVI measurements from AVHRR data for crop yield estimation and prediction. Int. J. Remote Sens. 14, 199–210.
Raes, D., Steduto, P., Hsiao, T.C., Fereres, E., 2009. AquaCrop—the FAO crop model to simulate yield response to water: II. Main algorithms and software description. Agron. J. 101, 438–447.
Rawlins, F., Ballard, S., Bovis, K., Clayton, A., Li, D., Inverarity, G., Lorenc, A., Payne, T., 2007. The Met Office global four-dimensional variational data assimilation scheme. Quarterly Journal of the Royal Meteorological Society: A journal of the atmospheric sciences, applied meteorology and physical oceanography 133, 347–362.
Reichle, R.H., Liu, Q., Koster, R.D., Crow, W.T., De Lannoy, G.J., Kimball, J.S., Kolassa, J., 2019. Version 4 of the SMAP Level-4 Soil Moisture Algorithm and Data. Product. 10, 3106–3130.
Reichle, R.H., De Lannoy, G.J., Liu, Q., Ardizzone, J.V., Colliander, A., Conaty, A., Koster, R.D., 2017. Assessment of the SMAP level-4 surface and root-zone soil moisture product using in situ measurements. J. Hydrometeorol. 18 (10), 2621–2645.
Rembold, F., Atzberger, C., Savin, I., Rojas, O., 2013. Using low resolution satellite imagery for yield prediction and yield anomaly detection. Remote Sensing 5, 1704–1733.
Ritchie, J., Singh, U., Godwin, D., & Hunt, L. (1989). A user's guide to CERES-Maize V2. 10. International Fertilizer Development Center, Muscle Shoals, AL.
Rivera, J., Verrelst, J., Leonenko, G., Moreno, J., 2013. Multiple cost functions and regularization options for improved retrieval of leaf chlorophyll content and LAI through inversion of the PROSAIL model. Remote Sensing 5, 3280–3304.
Roerink, G., Su, Z., Menenti, M., 2000. S-SEBI: A simple remote sensing algorithm to estimate the surface energy balance. Phys. Chem. Earth Part B 25, 147–157.
Rosema, A., Verhoef, W., Schroote, J., Snel, J., 1991. Simulating fluorescence light-canopy interaction in support of laser-induced fluorescence measurements. Remote Sens. Environ. 37, 117–130.
Rossi, C., Erten, E., 2014. Paddy-rice monitoring using TanDEM-X. IEEE Trans. Geosci. Remote Sens. 53, 900–910.
Rost, S., Gerten, D., Bondeau, A., Lucht, W., Rohwer, J., & Schaphoff, S. (2008). Agricultural green and blue water consumption and its influence on the global water system. Water resources research, 44.
Rötzer, K., Montzka, C., Entekhabi, D., Konings, A.G., McColl, K.A., Piles, M., Vereecken, H., 2017. Relationship Between Vegetation Microwave Optical Depth and Cross-Polarized Backscatter From Multiyear Aquarius Observations. IEEE J. Sel. Top. Appl. Earth Obs. Remote Sens.
Rouse Jr, J.W., Haas, R., Schell, J., & Deering, D. (1974). Monitoring vegetation systems in the Great Plains with ERTS.
Rudorff, B., Batista, G., 1990. Spectral response of wheat and its relationship to agronomic variables in the tropical region. Remote Sens. Environ. 31, 53–63.
Rundquist, D.C., Richard, H.O., Carlson, M.P., Cook, A.E., 1989. The Nebraska Center-Pivot Inventory: An example of operational satellite remote sensing on a long-term basis. Photogramm. Eng. Remote Sens 55, 587–590.
Salmon, J.M., Friedl, M.A., Frolking, S., Wisser, D., Douglas, E.M., 2015. Global rain-fed, irrigated, and paddy croplands: A new high resolution map derived from remote sensing, crop inventories and climate data. Int. J. Appl. Earth Obs. Geoinf. 38, 321–334.
Satalino, G., Mattia, F., Le Toan, T., Rinaldi, M., 2009. Wheat crop mapping by using ASAR AP data. IEEE Trans. Geosci. Remote Sens. 47, 527–530.
Scanlon, B.R., Faunt, C.C., Longuevergne, L., Reedy, R.C., Alley, W.M., McGuire, V.L., McMahon, P.B., 2012. Groundwater depletion and sustainability of irrigation in the US High Plains and Central Valley. Proc. Natl. Acad. Sci. 109, 9320–9325.
Scholes, R.J., & Biggs, R.A. (2004). Ecosystem services in southern Africa a regional assessment. CSIR.
Sellers, P., 1987. Canopy reflectance, photosynthesis, and transpiration, II. The role of biophysics in the linearity of their interdependence. Remote Sens. Environ. 21, 143–183.
Shanahan, J.F., Schepers, J.S., Francis, D.D., Varvel, G.E., Wilhelm, W.W., Tringe, J.M., Schlemmer, M.R., Major, D.J., 2001. Use of remote-sensing imagery to estimate corn grain yield. Agron. J. 93, 583–589.
Shao, Y., Campbell, J.B., Taff, G.N., Zheng, B., 2015. An analysis of cropland mask choice and ancillary data for annual corn yield forecasting using MODIS data. Int. J. Appl. Earth Obs. Geoinf. 38, 78–87.
Sharma, A., Hubert-Moy, L., Buvaneshwari, S., Sekhar, M., Ruiz, L., Bandyopadhyay, S., Corgne, S., 2018. Irrigation history estimation using multitemporal landsat satellite images: Application to an intensive groundwater irrigated agricultural watershed in India. Remote Sensing 10, 893.
Sharma, A.K., Hubert-Moy, L., Sriramulu, B., Sekhar, M., Ruiz, L., Bandyopadhyay, S., Mohan, S., Corgne, S., 2019. Evaluation of Radarsat-2 quad-pol SAR time-series images for monitoring groundwater irrigation. Int. J. Digital Earth 1–21.
Shi, J., Jackson, T., Tao, J., Du, J., Bindlish, R., Lu, L., Chen, K., 2008. Microwave vegetation indices for short vegetation covers from satellite passive microwave sensor AMSR-E. Remote Sens. Environ. 112, 4285–4300.
Shibayama, M., Takahashi, W., Morinaga, S., Akiyama, T., 1993. Canopy water deficit detection in paddy rice using a high resolution field spectroradiometer. Remote Sens. Environ. 45, 117–126.
Shiklomanov, I.A., Rodda, J.C., 2004. World water resources at the beginning of the twenty-first century. Cambridge University Press.
Shu, M., Zhou, L., Gu, X., Ma, Y., Sun, Q., Yang, G., Zhou, C., 2019. Monitoring of maize lodging using multi-temporal Sentinel-1 SAR data. Adv. Space Res.
Siebert, S., Burke, J., Faures, J.-M., Frenken, K., Hoogeveen, J., Döll, P., Portmann, F.T., 2010. Groundwater use for irrigation–a global inventory. Hydrol. Earth Syst. Sci. 14, 1863–1880.
Siebert, S., Kummu, M., Porkka, M., Döll, P., Ramankutty, N., Scanlon, B.R., 2015. A global data set of the extent of irrigated land from 1900 to 2005. Hydrol. Earth Syst. Sci. 19, 1521–1545.
Simonneaux, V., Duchemin, B., Helson, D., Er-Raki, S., Olioso, A., Chehbouni, A., 2008. The use of high-resolution image time series for crop classification and evapotranspiration estimate over an irrigated area in central Morocco. Int. J. Remote Sens. 29, 95–116.
Singh, D., Gupta, P., Pradhan, R., Dubey, A., Singh, R., 2016. Discerning shifting irrigation practices from passive microwave radiometry over Punjab and Haryana. J. Water Clim. Change 8, 303–319.
Singh, U., Ritchie, J.T., & Godwin, D. (1993). A User's Guide to CERES Rice, V2. 10. International Fertilizer Development Center Muscle Schoals.
Skakun, S., Franch, B., Vermote, E., Roger, J.-C., Becker-Reshef, I., Justice, C., Kussul, N., 2017. Early season large-area winter crop mapping using MODIS NDVI data, growing degree days information and a Gaussian mixture model. Remote Sens. Environ. 195, 244–258.
Somkuti, P., Bösch, H., Feng, L., Palmer, P.I., Parker, R.J., Quaife, T., 2020. A new space-borne perspective of crop productivity variations over the US Corn Belt. Agric. For. Meteorol. 281, 107826.
Srivastava, H.S., Patel, P., Navalgund, R.R., 2006. Application potentials of synthetic aperture radar interferometry for land-cover mapping and crop-height estimation. Curr. Sci. 00113891, 91.
Steduto, P., Hsiao, T.C., Raes, D., Fereres, E., 2009. AquaCrop—The FAO crop model to simulate yield response to water: I. Concepts and underlying principles. *Agronomy Journal* 101, 426–437.
Steele-Dunne, S.C., McNairn, H., Monsivais-Huertero, A., Judge, J., Liu, P.-W., Papathanassiou, K., 2017. Radar remote sensing of agricultural canopies: A review. IEEE J. Sel. Top. Appl. Earth Obs. Remote Sens. 10, 2249–2273.
Su, Z., 2002. The Surface Energy Balance System (SEBS) for estimation of turbulent heat fluxes. Hydrol. Earth Syst. Sci. 6, 85–100.
Sulser, T.B., Ringler, C., Zhu, T., Msangi, S., Bryan, E., Rosegrant, M.W., 2010. Green and blue water accounting in the Ganges and Nile basins: Implications for food and agricultural policy. J. Hydrol. 384, 276–291.
Tao, J., Wu, W., Liu, W., 2017. Spatial-Temporal Dynamics of Cropping Frequency in Hubei Province over 2001–2015. Sensors 17, 2622.
Tarantino, C., Casella, F., Adamo, M., Lucas, R., Beierkuhnlein, C., Blonda, P., 2019. Ailanthus altissima mapping from multi-temporal very high resolution satellite images. ISPRS J. Photogramm. Remote Sens. 147, 90–103.
Thenkabail, P., Dheeravath, V., Biradar, C., Gangalakunta, O.R., Noojipady, P., Gurappa, C., Velpuri, M., Gumma, M., Li, Y., 2009a. Irrigated area maps and statistics of India using remote sensing and national statistics. Remote Sensing 1, 50–67.

Thenkabail, P., GangadharaRao, P., Biggs, T., Krishna, M., Turral, H., 2007. Spectral matching techniques to determine historical land-use/land-cover (LULC) and irrigated areas using time-series 0.1-degree AVHRR pathfinder datasets. Photogramm. Eng. Remote Sens 73, 1029–1040.
Thenkabail, P., Ward, A., Lyon, J., 1994. Landsat-5 Thematic Mapper models of soybean and corn crop characteristics. Remote Sensing 15, 49–61.
Thenkabail, P.S., Biradar, C.M., Noojipady, P., Dheeravath, V., Li, Y., Velpuri, M., Gumma, M., Gangalakunta, O.R.P., Turral, H., Cai, X., 2009b. Global irrigated area map (GIAM), derived from remote sensing, for the end of the last millennium. Int. J. Remote Sens. 30, 3679–3733.
Thenkabail, P.S., Schull, M., Turral, H., 2005. Ganges and Indus river basin land use/land cover (LULC) and irrigated area mapping using continuous streams of MODIS data. Remote Sens. Environ. 95, 317–341.
Thenkabail, P.S., Smith, R.B., De Pauw, E., 2000. Hyperspectral vegetation indices and their relationships with agricultural crop characteristics. Remote Sens. Environ. 71, 158–182.
Thenkabail, P.S., Smith, R.B., De Pauw, E., 2002. Evaluation of narrowband and broadband vegetation indices for determining optimal hyperspectral wavebands for agricultural crop characterization. Photogramm. Eng. Remote Sens. 68, 607–622.
Thiruvengadachari, S., 1981. Satellite sensing of irrigation patterns in semiarid areas- An Indian study. Photogramm. Eng. Remote Sens. 47, 1493–1499.
Thorp, K., Tian, L., 2004. A review on remote sensing of weeds in agriculture. Precis. Agric. 5, 477–508.
Tian, S., Renzullo, L., Van Dijk, A., Tregoning, P., Walker, J., 2019. Global joint assimilation of GRACE and SMOS for improved estimation of root-zone soil moisture and vegetation response. Hydrology Earth System Science 23, 1067–1081.
Tilman, D., Balzer, C., Hill, J., Befort, B.L., 2011. Global food demand and the sustainable intensification of agriculture. Proc. Natl. Acad. Sci. 108, 20260–20264.
Tol, C., Verhoef, W., Timmermans, J., Verhoef, A., Su, Z., 2009. An integrated model of soil-canopy spectral radiances, photosynthesis, fluorescence, temperature and energy balance. Biogeosciences 6, 3109–3129.
Toomanian, N., Gieske, A., Akbary, M., 2004. Irrigated area determination by NOAA-Landsat upscaling techniques, Zayandeh river basin, Isfahan. Iran. *International journal of remote sensing* 25, 4945–4960.
Treuhaft, R.N., Cloude, S.R., 1999. The structure of oriented vegetation from polarimetric interferometry. IEEE Trans. Geosci. Remote Sens. 37, 2620–2624.
Treuhaft, R.N., Siqueira, P.R., 2000. Vertical structure of vegetated land surfaces from interferometric and polarimetric radar. Radio Sci. 35, 141–177.
Tsang, L., Ding, K.-H., Zhang, G., Hsu, C., Kong, J.A., 1995. Backscattering enhancement and clustering effects of randomly distributed dielectric cylinders overlying a dielectric half space based on Monte-Carlo simulations. IEEE Trans. Antennas Propag. 43, 488–499.
Tucker, C.J., 1979. Red and photographic infrared linear combinations for monitoring vegetation. Remote Sens. Environ. 8 (2), 127–150.
Tucker, C., Holben, B., Elgin Jr, J., McMurtrey III, J., 1980. Relationship of spectral data to grain yield variation. Photogramm. Eng. Remote Sens. 46, 657–666.
Tucker, C.J., Maxwell, E., 1976. Sensor design for monitoring vegetation canopies. Photogramm. Eng. Remote Sens. 42, 1399–1410.
Tuia, D., Verrelst, J., Alonso, L., Pérez-Cruz, F., Camps-Valls, G., 2011. Multioutput support vector regression for remote sensing biophysical parameter estimation. IEEE Geosci. Remote Sens. Lett. 8, 804–808.
Tuvdendorj, B., Wu, B., Zeng, H., Batdelger, G., Nanzad, L., 2019. Determination of Appropriate Remote Sensing Indices for Spring Wheat Yield Estimation in Mongolia. Remote Sensing 11, 2568.
Ulaby, F., Allen, C., Eger Iii, G., Kanemasu, E., 1984. Relating the microwave backscattering coefficient to leaf area index. Remote Sens. Environ. 14, 113–133.
Ulaby, F.T., Sarabandi, K., Mcdonald, K., Whitt, M., Dobson, M.C., 1990. Michigan microwave canopy scattering model. Int. J. Remote Sens. 11, 1223–1253.
Ullah, E., 1989. Mapping flowering Paterson's Curse (Echium plantagineum) around Lake Hume, north eastern Victoria, using Landsat TM data. Plant Prot Q 4, 155–157.
United Nations, U. (2015). Transforming Our World, the 2030 Agenda for Sustainable Development. General Assembly Resolution A/RES/70/1.
Van Diepen, C.v., Wolf, J., Van Keulen, H., & Rappoldt, C. (1989). WOFOST: a simulation model of crop production. Soil use and management, 5, 16-24.
van Dijk, A.I., Schellekens, J., Yebra, M., Beck, H.E., Renzullo, L.J., Weerts, A., Donchyts, G., 2018. Global 5 km resolution estimates of secondary evaporation including irrigation through satellite data assimilation. Hydrol. Earth Syst. Sci. 22, 4959–4980.
Veloso, A., Mermoz, S., Bouvet, A., Le Toan, T., Planells, M., Dejoux, J.-F., Ceschia, E., 2017. Understanding the temporal behavior of crops using Sentinel-1 and Sentinel-2-like data for agricultural applications. Remote Sens. Environ. 199, 415–426.
Velpuri, N., Thenkabail, P.S., Gumma, M.K., Biradar, C., Dheeravath, V., Noojipady, P., Yuanjie, L., 2009. Influence of resolution in irrigated area mapping and area estimation. Photogramm. Eng. Remote Sens. 75, 1383–1395.
Verhoef, W., 1984. Light scattering by leaf layers with application to canopy reflectance modeling: The SAIL model. Remote Sens. Environ. 16, 125–141.
Verhoef, W., Bach, H., 2003. Simulation of hyperspectral and directional radiance images using coupled biophysical and atmospheric radiative transfer models. Remote Sens. Environ. 87, 23–41.
Vermote, E.F., Tanré, D., Deuze, J.L., Herman, M., Morcette, J.-J., 1997. Second simulation of the satellite signal in the solar spectrum, 6S: An overview. IEEE Trans. Geosci. Remote Sens. 35, 675–686.
Verrelst, J., Rivera, J.P., Leonenko, G., Alonso, L., Moreno, J., 2013. Optimizing LUT-based RTM inversion for semiautomatic mapping of crop biophysical parameters from Sentinel-2 and-3 data: Role of cost functions. IEEE Trans. Geosci. Remote Sens. 52, 257–269.
Veysi, S., Naseri, A.A., Hamzeh, S., Bartholomeus, H., 2017. A satellite based crop water stress index for irrigation scheduling in sugarcane fields. Agric. Water Manag. 189, 70–86.
Vico, G., Porporato, A., 2015. Ecohydrology of agroecosystems: quantitative approaches towards sustainable irrigation. Bull. Math. Biol. 77 (2), 298–318.
Viña, A., Gitelson, A.A., Nguy-Robertson, A.L., Peng, Y., 2011. Comparison of different vegetation indices for the remote assessment of green leaf area index of crops. Remote Sens. Environ. 115, 3468–3478.
Wada, Y., Van Beek, L., Viviroli, D., Dürr, H.H., Weingartner, R., & Bierkens, M.F. (2011). Global monthly water stress: 2. Water demand and severity of water stress. Water resources research, 47.
Wada, Y., Van Beek, L.P., Van Kempen, C.M., Reckman, J.W., Vasak, S., & Bierkens, M.F. (2010). Global depletion of groundwater resources. Geophysical Research Letters, 37.
Wagle, P., Bhattarai, N., Gowda, P.H., Kakani, V.G., 2017. Performance of five surface energy balance models for estimating daily evapotranspiration in high biomass sorghum. ISPRS J. Photogramm. Remote Sens. 128, 192–203.
Wang, C., Wu, J., Zhang, Y., Pan, G., Qi, J., Salas, W.A., 2009. Characterizing L-band scattering of paddy rice in southeast China with radiative transfer model and multitemporal ALOS/PALSAR imagery. IEEE Trans. Geosci. Remote Sens. 47, 988–998.
Wang, J.R., Engman, E.T., Mo, T., Schmugge, T.J., Shiue, J., 1987. The effects of soil moisture, surface roughness, and vegetation on L-band emission and backscatter. IEEE Trans. Geosci. Remote Sens. 825–833.
Wang, L., Chang, Q., Yang, J., Zhang, X., Li, F., 2018. Estimation of paddy rice leaf area index using machine learning methods based on hyperspectral data from multi-year experiments. PLoS ONE 13, e0207624.
Wang, L.a., Zhou, X., Zhu, X., Dong, Z., & Guo, W. (2016). Estimation of biomass in wheat using random forest regression algorithm and remote sensing data. The Crop Journal, 4, 212-219.
Wiegand, C.L., Richardson, A.J., 1990. Use of spectral vegetation indices to infer leaf area, evapotranspiration and yield: I Rationale. Agro. J. 82, 623–629.
Wigneron, J.-P., Jackson, T., O'Neill, P., De Lannoy, G., De Rosnay, P., Walker, J., Ferrazzoli, P., Mironov, V., Bircher, S., Grant, J., 2017. Modelling the passive microwave signature from land surfaces: A review of recent results and application to the L-band SMOS & SMAP soil moisture retrieval algorithms. Remote Sens. Environ. 192, 238–262.
Wichelns, D., Qadir, M., 2015. Achieving sustainable irrigation requires effective management of salts, soil salinity, and shallow groundwater. Agric. Water Manag. 157, 31–38.
Williams, J., Jones, C., Kiniry, J., Spanel, D.A., 1989. The EPIC crop growth model. Transactions of the ASAE 32, 497–0511.
Wiseman, G., McNairn, H., Homayouni, S., Shang, J., 2014. RADARSAT-2 polarimetric SAR response to crop biomass for agricultural production monitoring. IEEE J. Sel. Top. Appl. Earth Obs. Remote Sens. 7, 4461–4471.
Wisser, D., Frolking, S., Douglas, E.M., Fekete, B.M., Vörösmarty, C.J., Schumann, A.H., 2008. Global irrigation water demand: Variability and uncertainties arising from agricultural and climate data sets. Geophys. Res. Lett. 35.
Wu, C., Niu, Z., Tang, Q., Huang, W., 2008. Estimating chlorophyll content from hyperspectral vegetation indices: Modeling and validation. Agric. For. Meteorol. 148, 1230–1241.
Wulder, M.A., White, J.C., Coops, N.C., Butson, C.R., 2008. Multi-temporal analysis of high spatial resolution imagery for disturbance monitoring. Remote Sens. Environ. 112, 2729–2740.
Wylie, B., Harrington Jr, J., Prince, S., Denda, I., 1991. Satellite and ground-based pasture production assessment in Niger: 1986–1988. Int. J. Remote Sens. 12, 1281–1300.
Xiang, K., Ma, M., Liu, W., Dong, J., Zhu, X., Yuan, W., 2019. Mapping Irrigated Areas of Northeast China in Comparison to Natural Vegetation. Remote Sensing 11, 825.
Xiao, X., Boles, S., Liu, J., Zhuang, D., Frolking, S., Li, C., Salas, W., Moore III, B., 2005. Mapping paddy rice agriculture in southern China using multi-temporal MODIS images. Remote Sens. Environ. 95, 480–492.
Yan, K., Park, T., Chen, C., Xu, B., Song, W., Yang, B., Zeng, Y., Liu, Z., Yan, G., Knyazikhin, Y., 2018. Generating global products of lai and fpar from snpp-viirs data: Theoretical background and implementation. IEEE Trans. Geosci. Remote Sens. 56, 2119–2137.
Yang, H., Chen, E., Li, Z., Zhao, C., Yang, G., Pignatti, S., Casa, R., Zhao, L., 2015. Wheat lodging monitoring using polarimetric index from RADARSAT-2 data. Int. J. Appl. Earth Obs. Geoinf. 34, 157–166.
Yoon, S.Y., Lee, S.-K., & Won, J.-S. (2017). Rice paddy height estimation from single-polarization TanDEM-X science phase data. In, 2017 IEEE International Geoscience and Remote Sensing Symposium (IGARSS) (pp. 930-933): IEEE.
Yuan, L., Bao, Z., Zhang, H., Zhang, Y., Liang, X., 2017. Habitat monitoring to evaluate crop disease and pest distributions based on multi-source satellite remote sensing imagery. Optik 145, 66–73.
Yuan, L., Zhang, J., Shi, Y., Nie, C., Wei, L., Wang, J., 2014. Damage mapping of powdery mildew in winter wheat with high-resolution satellite image. Remote sensing 6, 3611–3623.
Yueh, S.H., Kong, J.A., Jao, J.K., Shin, R.T., Le Toan, T., 1992. Branching model for vegetation. IEEE Trans. Geosci. Remote Sens. 30, 390–402.
Yuzugullu, O., Erten, E., Hajnsek, I., 2016. Estimation of rice crop height from X-and C-band PolSAR by metamodel-based optimization. IEEE J. Sel. Top. Appl. Earth Obs. Remote Sens. 10, 194–204.
Zaussinger, F., Dorigo, W., Gruber, A., Tarpanelli, A., Filippucci, P., Brocca, L., 2019. Estimating irrigation water use over the contiguous United States by combining satellite and reanalysis soil moisture data. Hydrol. Earth Syst. Sci. 23, 897–923.
Zebker, H.A., Villasenor, J., 1992. Decorrelation in interferometric radar echoes. IEEE Trans. Geosci. Remote Sens. 30, 950–959.
Zhang, J., Huang, Y., Pu, R., Gonzalez-Moreno, P., Yuan, L., Wu, K., Huang, W., 2019. Monitoring plant diseases and pests through remote sensing technology: A review.

Comput. Electron. Agric. 165, 104943.
Zhang, J., Huang, Y., Yuan, L., Yang, G., Chen, L., Zhao, C., 2016. Using satellite multispectral imagery for damage mapping of armyworm (Spodoptera frugiperda) in maize at a regional scale. Pest Manag. Sci. 72, 335–348.
Zhang, J., Pu, R., Yuan, L., Huang, W., Nie, C., Yang, G., 2014a. Integrating remotely sensed and meteorological observations to forecast wheat powdery mildew at a regional scale. IEEE J. Sel. Top. Appl. Earth Obs. Remote Sens. 7, 4328–4339.
Zhang, J., Pu, R., Yuan, L., Wang, J., Huang, W., Yang, G., 2014b. Monitoring powdery mildew of winter wheat by using moderate resolution multi-temporal satellite imagery. PLoS ONE 9, e93107.
Zhang, N., Hong, Y., Qin, Q., Liu, L., 2013. VSDI: a visible and shortwave infrared drought index for monitoring soil and vegetation moisture based on optical remote sensing. Int. J. Remote Sens. 34, 4585–4609.
Zhang, X., Qiu, J., Leng, G., Yang, Y., Gao, Q., Fan, Y., Luo, J., 2018. The potential utility of satellite soil moisture retrievals for detecting irrigation patterns in China. Water 10, 1505.
Zhao, D., Huang, L., Li, J., Qi, J., 2007. A comparative analysis of broadband and narrowband derived vegetation indices in predicting LAI and CCD of a cotton canopy. ISPRS J. Photogramm. Remote Sens. 62, 25–33.
Zhao, F., Dai, X., Verhoef, W., Guo, Y., van der Tol, C., Li, Y., Huang, Y., 2016. FluorWPS: A Monte Carlo ray-tracing model to compute sun-induced chlorophyll fluorescence of three-dimensional canopy. Remote Sens. Environ. 187, 385–399.
Zhao, L., Yang, J., Li, P., Shi, L., Zhang, L., 2017. Characterizing lodging damage in wheat and canola using radarsat-2 polarimetric SAR Data. Remote Sensing Letters 8, 667–675.
Zheng, Q., Huang, W., Cui, X., Shi, Y., Liu, L., 2018. New spectral index for detecting wheat yellow rust using Sentinel-2 multispectral imagery. Sensors 18, 868.
Zohaib, M., Kim, H., Choi, M., 2019. Detecting global irrigated areas by using satellite and reanalysis products. Sci. Total Environ. 677, 679–691.